AN ABSTRACT OF THE THESIS OF

GERALD GEORGE CONNARD for the degree of MASTER OF SCIENCE

in Geophysics presented on November 16, 1979

Title: ANALYSIS OF AEROMAGNETIC MEASUREMENTS FROM THE CENTRAL OREGON CASCADES

Abstract approved: Redacted for Privacy

Dr. Richard Couch

To assist in the assessment of potential geothermal resources, the Geophysics Group at Oregon State University conducted an aeromagnetic survey of the Central Oregon Cascades from 43°00' to 44°15'N and 121°00' to 122°30'W. This area includes three major centers of Holocene silicic volcanism and extends from the Basin and Range province in the east to the transition zone between the Western and High Cascades mountain ranges in the west. The aeromagnetic data was obtained using a high quality transponder navigation system to accurately locate the position of each measurement and a magnetic base station to monitor the diurnal magnetic variation for removal from the survey, values. These survey techniques yielded 60,000 data points with an RMS uncertainty of only 4.2 gammas.

Fourier transformation of the two-dimensional aeromagnetic anomaly data provides a frequency domain representation, or spectrum of the data which is useful for depths-to-

source and Curie point isotherm depth calculations. The frequency domain representation also facilitates low-pass filtering of the magnetic anomaly data to enhance regional trends. When wavelengths shorter than 15 km are suppressed, the resulting map shows a number of northwest-southeast trends in the anomalies, particularly in the southeast portion of the area. Suppressing the wavelengths shorter than 25 km reveals a north 25° east trend along the eastern side of the High Cascades which is obscured by the northwest-southeast trends prominent in the unfiltered anomaly map.

The magnetic source depth calculations show that the depth of the magnetic basement in the survey area varies from as deep as 6 km below sea level in the northwest portion of the area where the terrain averages 1.1 km above sea level, to sea level in the southern half of the area where the terrain averages 1.5 km above sea level.

Only four of nine subdivisions of the study area yield estimates of the lower boundaries of the crustal magnetized layer which relate to the Curie point isotherm depths. Spectra from the other five subdivisions do not produce source bottom depths, possibly because the Curie point isotherm is too deep to have an influence on the low frequency part of the spectrum, or because sources with large horizontal dimensions may mask the low frequency effects of source bottoms. The calculations show an elongate zone

of elevated Curie point isotherm depths extending from the Crater Lake area to Bend, Oregon and averaging 9 to 12 km below sea level. Assuming a Curie temperature of 580°C (the Curie point of magnetite), these shallow Curie depths predict temperature gradients greater than 50°C/km and surface heat flow values greater than 100 m W/m^2. The limited heat flow data available in the area support these conclusions.

Analysis of Aeromagnetic Measurements from the Central Oregon Cascades

by

Gerald George Connard

A THESIS

submitted to

Oregon State University

in partial fulfillment of
the requirements for the
degree of

Master of Science

Completed November, 1979

Commencement June, 1980

APPROVED:

Redacted for Privacy

Associate Professor of Geophysics
in charge of major

Redacted for Privacy

Dean of the School of Oceanography

Redacted for Privacy

Dean of the Graduate School

Date thesis is presented November 16, 1979

Typed by Deanna L. Cramer for Gerald George Connard

ACKNOWLEDGEMENTS

I would like to thank my major professor and advisor Dr. Richard Couch for his support, advice, and patience. Dr. Richard Blakely introduced me to the problem addressed in this thesis and provided advice and moral support whenever possible. Everyone in the Geophysics Group at OSU helped me in one way or another with this work, particularly Mike Gemperle, Fran Boler, Steve Pitts, Jeb Bowers, Darcy Burt, and Steve Troseth.

I wish to thank Dr. Steve Johnson and Gordon Ness for critically reading the manuscript and offering their comments and criticisms. Gordon also helped preserve my sanity during times of stress.

Throughout this work my wife Christie provided support, patience, and motivation when I needed it the most.

The research was funded by U.S. Geological Survey contract number 14-08-0001-G-393. During part of my stay at Oregon State University I received financial assistance from a Texaco Fellowship.

TABLE OF CONTENTS

LIST OF FIGURES

List of Figures -- continued

LIST OF TABLES

ANALYSIS OF AEROMAGNETIC MEASUREMENTS FROM THE CENTRAL OREGON CASCADES

INTRODUCTION

Under the auspices of the Geothermal Steam Act of 1970, Goodwin et al. (1971) designated the High Cascade portion of the Cascade Mountain Range as an "area valuable prospectively" for geothermal resources. In 1975, supported by the U.S. Geologic Survey Extramural Geothermal Program, the Geophysics Group at the School of Oceanography, Oregon State University, conducted a detailed aeromagnetic survey of the area between 43° to 44°14'N latitude and 121° to 120°30'W longitude to further assess the geothermal potential. As shown in Figure 1, the study area includes three major centers of Holocene silicic volcanism: the Three Sisters, Newberry Crater, and Crater Lake. It extends from the Basin and Range province in the east to the transition zone between the Western and High Cascades in the west.

There are numerous surface manifestations of geothermal heat at shallow depth within the study area. Bowen et al. (1978) lists 12 thermal springs located along the boundary between the Western and High Cascades and in Newberry Crater. Blackwell et al. (1978) also show surface heat flow values over 100 mW/m^2 throughout much of the area,

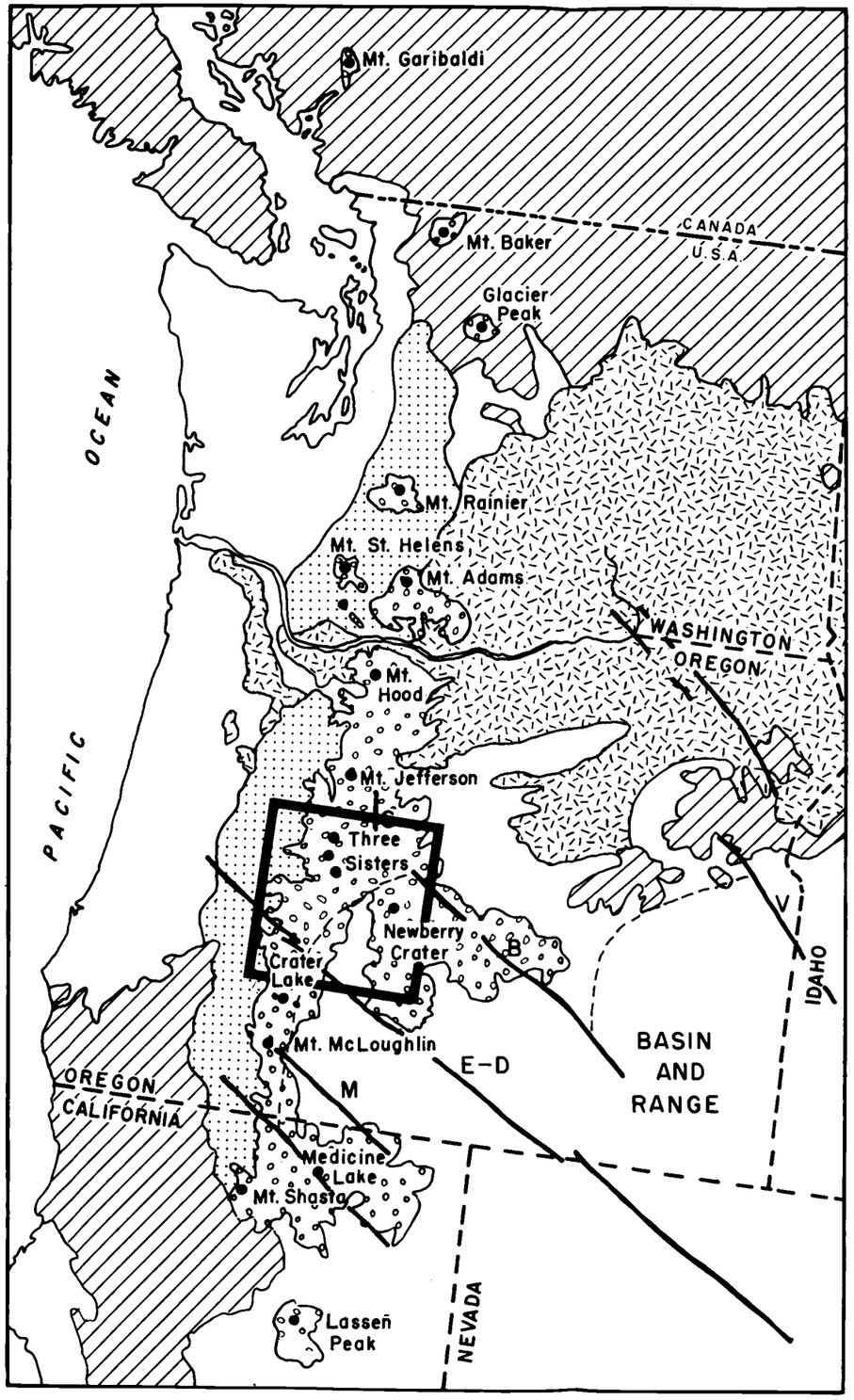

QUATERNARY VOLCANIC ROCKS

WESTERN CASCADES

COLUMBIA RIVER BASALTS

PRE-TERTIARY ROCKS

---- Boundary of Basin and Range

• Quaternary volcanic centers

—— Fault zones:

B = Brothers Fault Zone
E-D = Eugene-Denio Zone
M = McLoughlin Zone
V = Vale Zone
S = Sisters Fault Zone

Generalized geology after McBirney (1968).
Fault data after Lawrence (1976).

Figure 1

while according to Stacey (1977) the average heat flow for Mesozoic and Cenozoic orogenic areas is 61 mW/m^2.

The objective of this study is the reduction, and interpretation of the aeromagnetic data to clarify the regional tectonic and thermal framework of the survey area. Because of the geologic complexity of the study area it is difficult to isolate magnetic anomalies caused by individual sources. However, it is possible to calculate the depth of an ensemble of magnetic sources and the average thickness of those sources using spectral analysis (Spector and Grant, 1970; Shuey et al., 1977). Estimates of Curie point isotherm depths may be made using this depth and thickness information. Since the Curie point is the temperature at which rocks lose their ferromagnetic properties, it provides a link between magnetic anomaly data and thermal models. This study also uses spectral analysis techniques to suppress high frequency components observed in the magnetic anomaly data. The resulting low-pass filtered maps reveal deeper structural trends in the area which are obscured in the unfiltered magnetic anomaly map. The results of this study, which used magnetic anomaly trend analysis, magnetic source depth calculations, and the Curie point depth estimates, suggest a zone of high subsurface temperatures under the High Cascades at relatively shallow depths.

GEOLOGY AND PHYSIOGRAPHY OF THE CENTRAL CASCADES OF OREGON

Three of the major physiographic provinces of Oregon identified by Dicken (1965) are partially included in the Central Oregon Cascades study area: the Western and High Cascades, the Basin and Range, and the High Lava Plains. Figure 2 shows the topography of the area in 305 meter (1,000 foot) contours. The Western Cascades appear along the western edge of the topographic map as an area of steep, east-west ridges and valleys which form the upper drainage for the McKenzie, Willamette, and Umpqua rivers. The High Cascades subprovince appears just east of the Western Cascades and is generally over 1,500 meters (5,000 feet) in elevation. The Basin and Range Province appears in the southeastern quadrant and the High Lava Plains occupy the east and northeast portions of the area. The highest elevations occur at Newberry Crater in the east and in the High Cascades where South Sister reaches 3,160 meters (10,358 feet). The lowest elevations occur in the river valleys of the Western Cascades. There the McKenzie River is at 300 meters (1,000 feet) elevation.

The Cascade Range in Oregon occupies a broad, north trending structural depression, or graben, in older rock (Peck et al., 1964; Allen, 1965; Taylor, 1973, 1978; and others). The Western Cascades consist mainly of Late Eocene to Late Miocene volcanic flows, tuffs, and tuffaceous

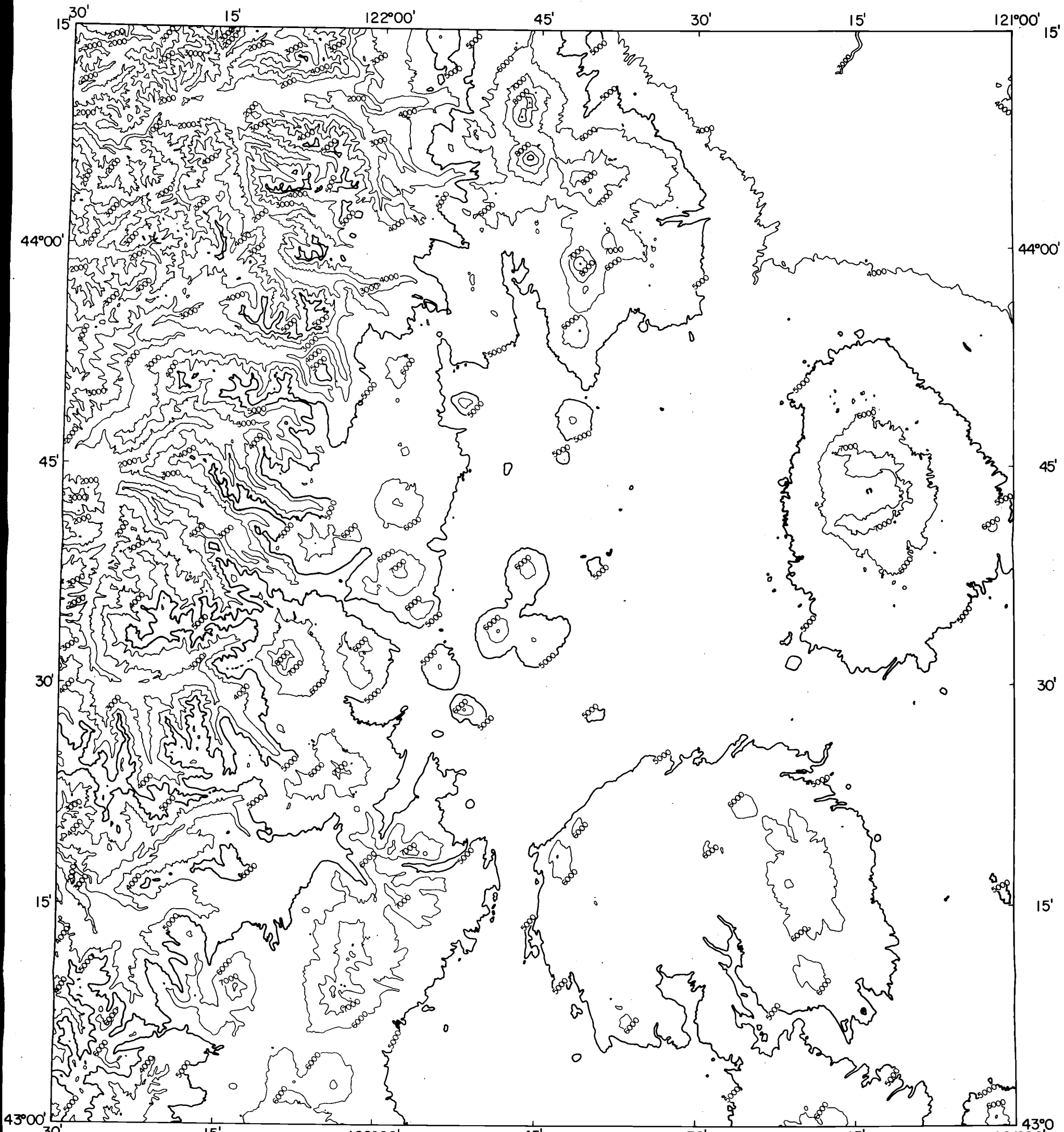

TOPOGRAPHIC MAP
CASCADE MOUNTAIN RANGE, CENTRAL OREGON

DATA FROM U.S.G.S 1:250,000 QUADRANGLE MAPS
BEND NL 10-12
CRESCENT NK 10-3
ROSEBURG NK 10-2
SALEM NL 10-11

KILOMETERS
0 5 10 15 20
0 5 10
MILES

UNIVERSAL TRANVERSE MERCATOR PROJECTION
CONTOUR INTERVAL 1000 FEET
SCALE 1:500,000

FIGURE 2

OREGON STATE UNIVERSITY
JANUARY, 1978

sediments thought by Peck et al. (1964) to overlie the Ecocene marine sedimentary deposits and basal flows of the Umpqua, Tyee, and Spencer formations. Peck et al. (1964) divided the volcanic flows and tuffs of the Western Cascades into three main groups: the Late Eocene Colestin Formations, the Oligocene and Early Miocene Little Butte Volcanics, and the Late Miocene Sardine Formations.

Rocks of the High Cascades unconformably overlie part of the folded and faulted Western Cascades. Callagham and Buddington (1938) and Baldwin (1976) have proposed that the High Cascades were emplaced on the eastern, downdropped side of a large north-trending fault system. The presence of other faults downthrown to the west on the eastern side of the High Cascades at Green Ridge (Wells and Peck, 1961) and Walker Rim (Peterson and McIntyre, 1970) suggests that the High Cascades occupy a graben structure superimposed on the structure of the Cascades range as a whole. The High Cascades Quaternary andesitic strato-volcanoes are built on large basaltic to basaltic andesite shields of Plio-Plistocene lavas and tuffs (Williams, 1957). The volcanoes in the study area are divergent; the extrusives are primarily siliceous andesite or dacite, but they also exhibit very basaltic and rhyolitic phases (McBirney, 1968).

The Basin and Range province extends from New Mexico and Arizona, through Utah and Nevada, to the High Cascades and High Lava Plains in Oregon. Much of the structure and

stratigraphy of the Basin and Range province within this study area are masked by the Quaternary Stams Mountain volcanics and ash from Mt. Mazama. Volcanic activity in the Basin and Range province, characterized by rhyolite flows, ash flow tuffs, and andesites, appears to be associated with the subduction of oceanic crust beneath western North America prior to 19 million years b.p. (Scholz et al., 1971; Smith, 1977). Bi-modal basaltic-rhyolitic volcanism, followed by crustal extension, began at about 15 million years b.p. and continues to the present (Smith, 1977).

The sediment-filled La Pine Valley separates the High Lava Plains structure of Newberry Crater from the High Cascades. The High Lava Plains province consists of relatively undeformed lavas, tuffs, and alluvium, with numerous cinder cones, lava tubes and other surface expressions of recent volcanism. The formations are predominantly Pliocene and Pleistocene, few of which have been formally named or described (Baldwin, 1976). MacLeod et al. (1975) describe a well-defined monotonic age progression of rhyolitic domes ranging from about 10 million years b.p. in easternmost Oregon, to less than 1 million years on the west flank of the Newberry Crater.

TOTAL FIELD MAGNETIC ANOMALY MAPS

During May and June of 1977, personnel from the Geophysics group at Oregon State University conducted an aeromagnetic survey in the area between 43° and 44°15'N latitude and 121° and 122°30'W longitude. Figure 3 shows a map of 16,000 km of flight lines flown at 2.74 km (9,000 feet) above sea level (ASL) over the region. A flight elevation of 2.74 km ASL allowed almost the entire area to be covered at one observation level with a minimum terrain clearance. As shown in Figure 3 the summits of Mt. Thielson and Bachelor Butte extend slightly above 2.74 km but did not interrupt the flight line pattern. However, the summits of the Three Sisters which extend to over 3 km and Broken Top at 2.8 km caused significant "holes" in the flight lines at the flight elevation of 2.74 km. Therefore, the 1,000 km of flight lines shown in Figure 4 were flown at 3.35 km (11,000 feet) ASL to obtain data over the higher topography of the Three Sisters area. These lines extend well beyond the Three Sisters-Broken Top area to provide adequate overlap of the measurements made at 2.74 km. The distance between the east-west traverses, at both elevations was 1.61 km (one statute mile). Spacing between the north-south tie-lines was 8.05 km (five statute miles). The entire survey yielded a total of 60,000 data points,

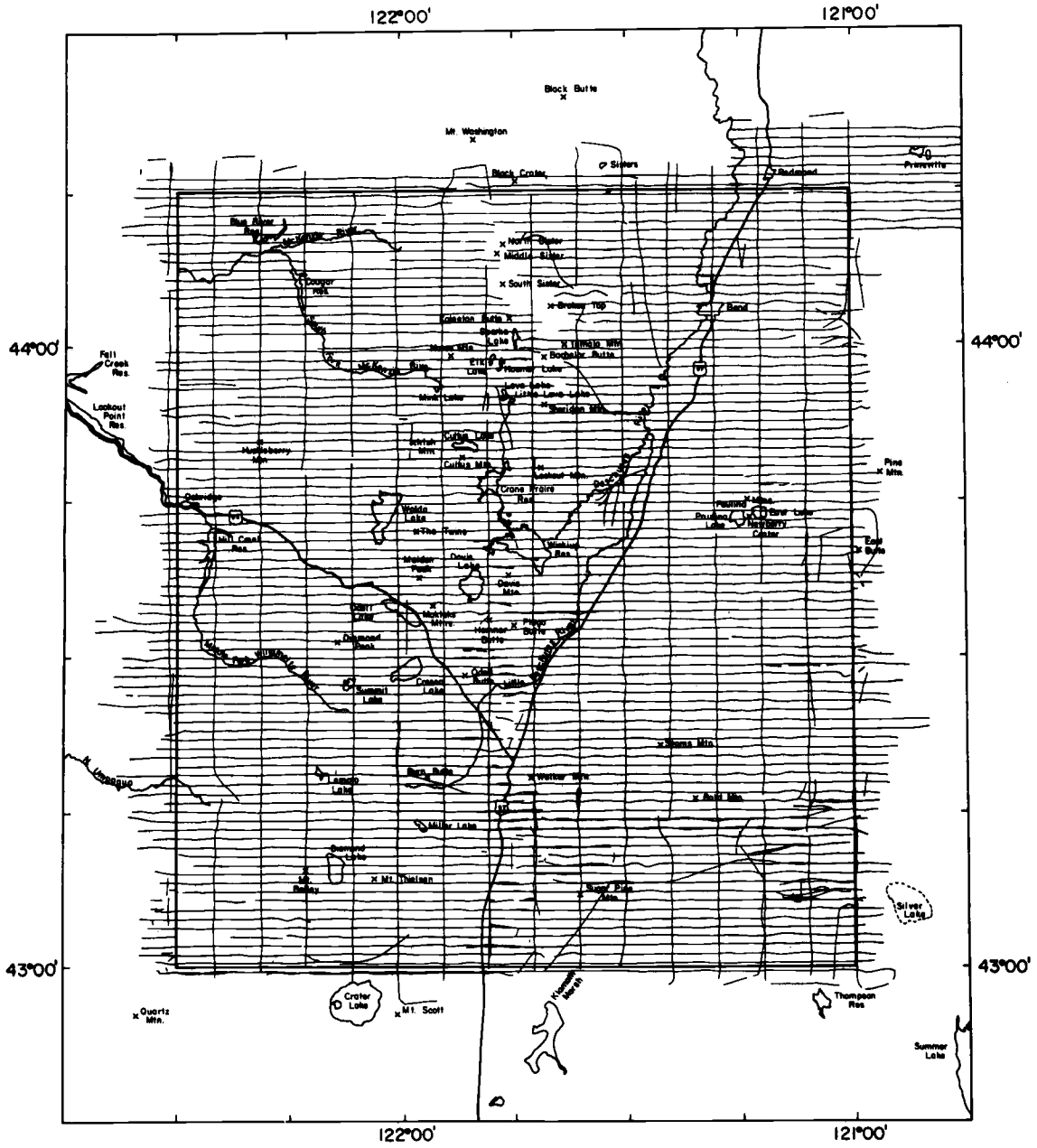

CASCADES AEROMAGNETIC FLIGHT LINES
FLIGHT ELEVATION 9,000 FEET
OREGON STATE UNIVERSITY, DECEMBER, 1977

Figure 3. Flightlines of the Central Oregon Cascades aeromagnetic survey obtained at 9,000 feet.

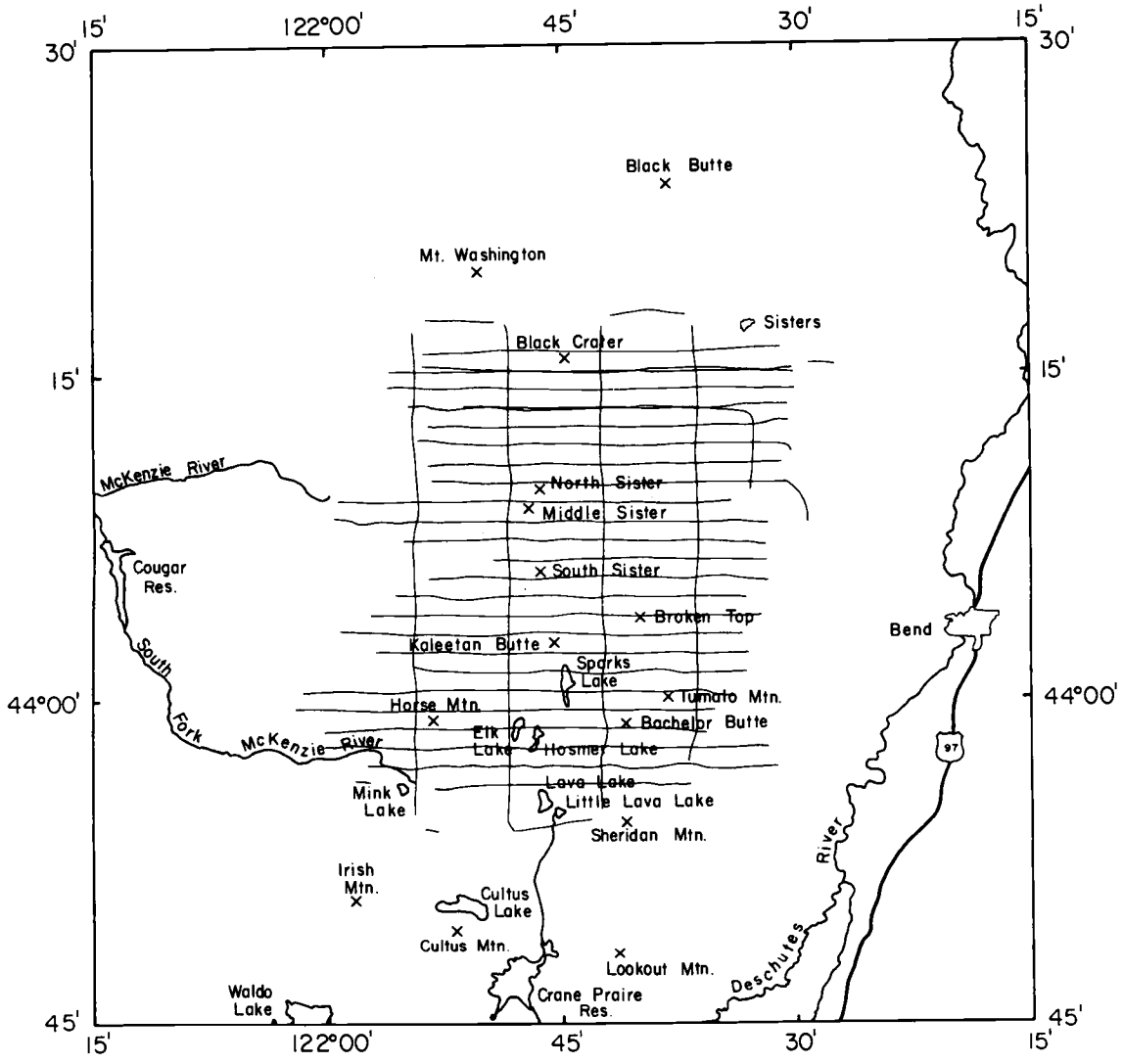

CASCADES AEROMAGNETIC FLIGHT LINES

FLIGHT ELEVATION 11,000 FEET

OREGON STATE UNIVERSITY, DECEMBER, 1977

Figure 4. Flightlines of the Central Oregon Cascades aeromagnetic survey obtained at 11,000 feet.

spaced at intervals of approximately 300 meters along the flight lines.

Figure 5 shows the total field aeromagnetic anomalies of the Central Cascades study area prepared from the data collected at an elevation of 2.74 km ASL and Figure 6 shows the total field aeromagnetic anomaly map of the Three Sisters area prepared from the data collected at 3.35 km ASL. Both maps are contoured at 50 gamma (nanotesla) intervals and have the regional geomagnetic field (IGRF 75) and the effects of diurnal magnetic variations removed. A radar transponder navigation system provided horizontal positions for the survey accurate to ±15 meters (see Appendix B). This precise navigation combined with the careful monitoring of diurnal changes of the geomagnetic field at a base station located at Sunriver, Oregon produced very small crossing errors. The RMS uncertainty of individual data points is 4.2 gammas.

A number of the short wavelength magnetic anomalies in Figure 5 correlate well with the topography, particularly the circular positive anomalies associated with the young volcanic cones of the High Cascades. Low amplitude long wavelength anomalies occur in the northeast corner and along the western edge of the survey area where the average topographic elevation is less than 1.3 km. Table 1 lists the topographic features that correlate with prominent anomalies on the 2.74 km observation level map

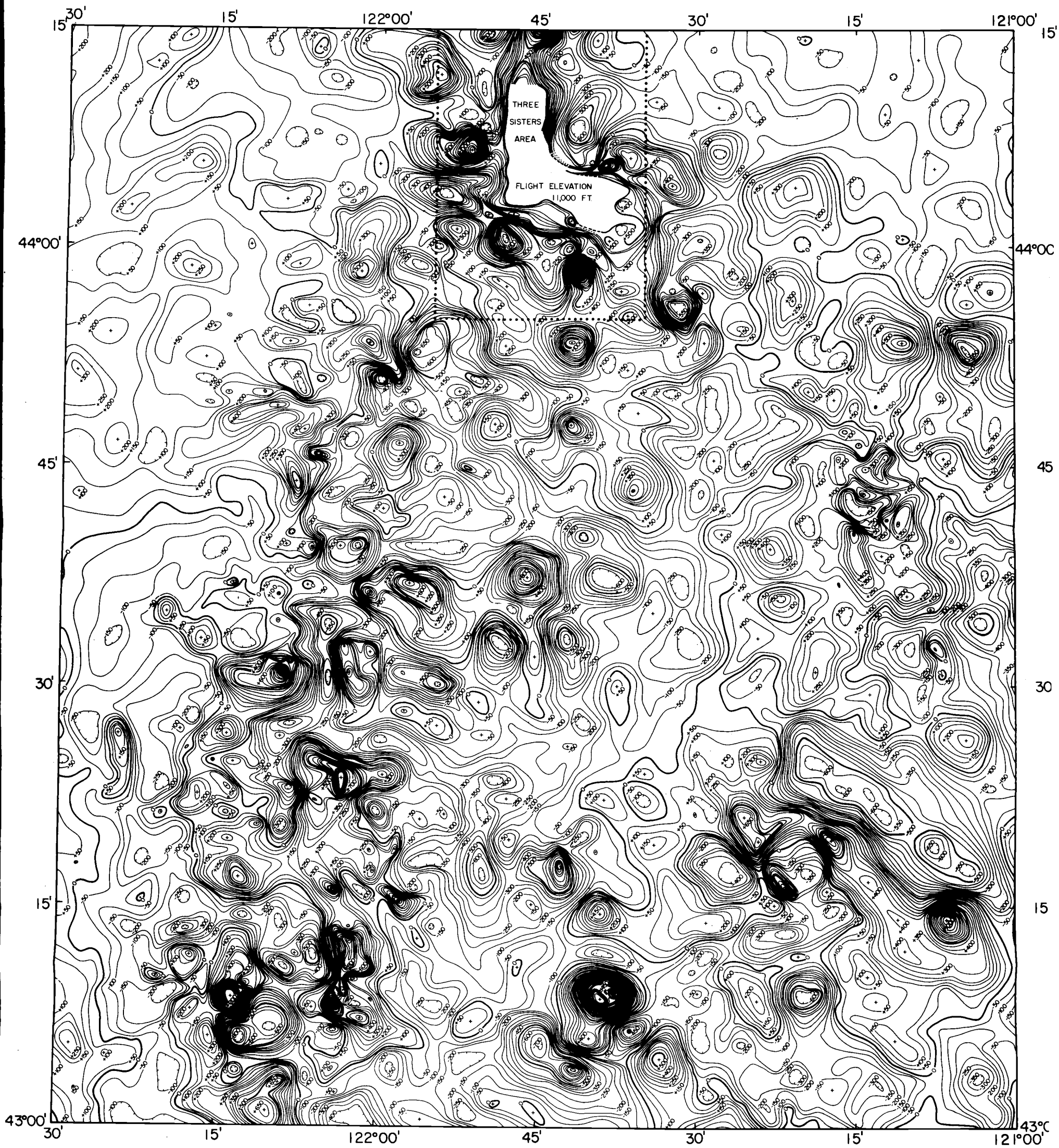

TOTAL FIELD AEROMAGNETIC ANOMALY MAP
CASCADE MOUNTAIN RANGE, CENTRAL OREGON

KILOMETERS
0 5 10 15 20
0 5 10
MILES

TOTAL FIELD DATA FROM:
GEOPHYSICS GROUP, OSU, 1977
I.G.R.F. 1975
FLIGHT ELEVATION 9,000 FT.

UNIVERSAL TRANSVERSE MERCATOR PROJECTION
CONTOUR INTERVAL 50 GAMMAS
ESTIMATED RMS UNCERTAINTY 4 GAMMAS
SCALE 1:500,000

OREGON STATE UNIVERSITY
FEBRUARY, 1978

FIGURE 5

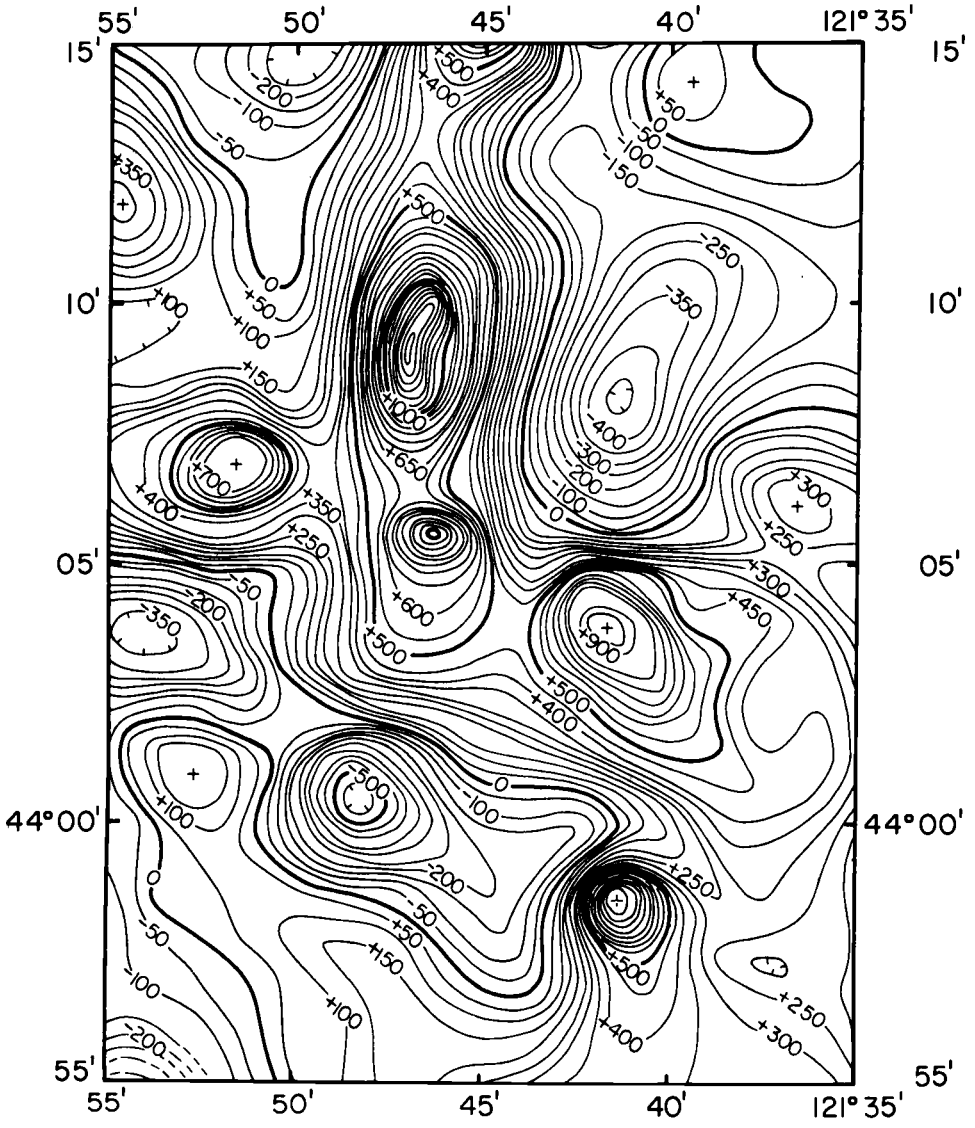

TOTAL FIELD AEROMAGNETIC ANOMALY MAP

THREE SISTERS AREA, CENTRAL OREGON

TOTAL FIELD DATA FROM:
GEOPHYSICS GROUP, OSU, 1977
I.G.R.F. 1975
FLIGHT ELEVATION 11,000 FT.

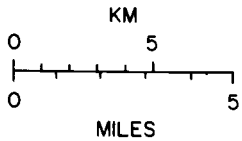

UTM PROJECTION
CONTOUR INTERVAL 50 GAMMAS
EST. RMS UNCERTAINTY 4 GAMMAS

OREGON STATE UNIVERSITY
FEBRUARY, 1978

Figure 6. Total field aeromagnetic anomaly map of the Three Sisters area.

Table 1. Physiographic features and associated magnetic anomalies on the 2.74 km observation level map.

Physiographic Features	Location	Elevation (meters)	Anomaly Value (gammas)
Bachelor Butte	43°59'/121°41'	2,760	+1,900
Mt. Bailey	43°09'/122°13'	2,550	+1200/-800
Bald Mt.	43°16'/121°21'	2,270	-750
Cowhorn Mt.	43°24'/122°03'	2,340	+1,000
Cryder Butte	43°34'/121°43'	1,650	-600
Davis Mt.	43°38'/121°46'	2,020	+800
Diamond Peak	43°31'/122°09'	2,670	+1,200
Gilchrist Butte	43°38'/121°40'	1,680	-600
Hamner Butte	43°34'/121°49'	2,160	-550
Horse Ridge	43°53'/121°04'	1,520	-650
Lookout Mt.	43°48'/121°42'	1,900	-600
Paulina Peak	43°41'/121°51'	2,430	+500
Mt. Ray	43°40'/122°03'	2,130	-700
Round Butte	43°05'/121°41'	1,650	-900
Royce Mt.	43°31'/121°54'	1,850	-600
Sheridan Mt.	43°31'/121°41'	2,130	+1,050
Stams Mt.	43°22'/121°26'	1,990	+650
Sugarpine Mt.	43°07'/121°36'	1,960	-500
Mt. Thielson	43°09'/122°04'	2,800	+1,100
Walker Mt.	43°18'/121°43'	2,160	-960

and Table 2 lists features appearing on the 3.35 km observation level map.

In Figure 5 a maximum amplitude of +1,900 gammas occurs in the positive anomaly associated with Bachelor Butte at 43°59'N latitude and 121°43'W longitude. Because the nearest flightline passed within a few hundred meters of the summit, this high value is reasonable. On the Three Sisters area map, the anomaly associated with Bachelor Butte is less than 1,000 gammas. The lowest anomaly value of -960 gammas occurs over Walker Mountain at 43°18'N latitude and 121°43'W longitude. However, Walker Rim, the fault scarp striking northeast from Walker Mountain has little or no magnetic expression.

When terrain clearance is considered, the most prominent anomaly is the pronounced circular high at 43°06'N and 121°36'W which reaches a maximum of 1,700 gammas. The highest elevation in this area is 1,960 meters at Sugarpine Mountain, 10 km southeast of the center of the anomaly. Geologic maps of the area (Peterson and McIntyre, 1970) give no indication of the source for this anomaly. Our field investigation in the area revealed a vertical dike of andesite approximately 30 meters wide which suggests the possibility of other large intrusive bodies near the surface.

The relatively low amplitude of the anomalies associated with Newberry Crater (located on the east side of

Table 2. Physiographic features and associated magnetic anomalies on the 3.35 km observation level map.

Physiographic Feature	Location	Elevation (meters)	Anomaly Value (gammas)
Bachelor Butte	43°59'/121°41'	2,760	+900
Broken Top	44°05'/121°42'	2,800	+900
North-Middle Sister	44°09'/121°47'	3,070	+1,350
South Sister	44°06'/121°46'	3,160	+1,000

Figure 3) is surprising for such a large feature. Near the south rim where elevations reach almost 2,500 meters, there is a maximum anomaly of only 500γ, which then decreases to a crescent-shaped low of -150γ inside the crater.

Other peaks that have little or no magnetic expression include Cultus Mountain at 43°49'N latitude, 121°52'W longitude with an elevation of 2,060 meters; Odell Butte at 43° 28'N latitude, 121°2'W longitude, a 2,190 meter peak at the southeast edge of the study area; and the Twins, at 43°1'N latitude, 121°2'W longitude, a 2,190 meter young volcanic cone which lies at the crest of the High Cascades.

North of Newberry Crater, a distinctive positive and negative anomaly pair occurs with peak values of +600 gammas and -650 gammas separated by 5 km. As listed in Table 1, the negative half of this pair of anomalies correlates well with the Pliocene horst named Horse Ridge, where normal faults of the Brothers Fault zone, described by Walker (1969) and Peterson et al. (1976), strike northwest-southeast. The positive half occurs over flat terrain; however, Peterson et al. (1976), mapped "mafic vent rocks" in the area at the Arnold Ice Cave lava tube.

South of the Brothers Fault zone, typical northwest-southeast basin and range trends appear in the anomalies. Beginning at the eastern boundary of the study area near 43°15'N latitude, a prominent broad negative anomaly, with a minimum of less than -600 gammas, extends northeast

through Fort Rock Valley and ends abruptly before reaching the La Pine valley. This anomaly minimum is coincident with the western end of a zone of Pliocene maars (explosive tuff rings) described by Peterson and Groh (1963) and occurs just north of, and is parallel to, the Eugene-Denio lineament described by Lawrence (1976). Here, between the Fort Rock Valley and the Eugene-Denio lineation, the anomalies exhibit characteristic criss-cross patterns similar to that observed by Donath (1958, 1962) in the Summer Lake area, and by Lawrence (1976) throughout the Basin and Range Province in Oregon. Pitts (1979) found the same trends in his Residual Gravity Anomaly Map in this area.

The short wavelength magnetic anomalies associated with the High Cascades show a definite right-lateral offset near 43°30'N latitude. This is consistent with Lawrence's (1976) proposal that the Eugene-Denio lineation crosses the Cascade Range at Willamette Pass and causes a 10-20 km offset in the High Cascades trend. This offset is more apparent in the magnetic anomaly pattern than on the topographic map.

Another parallel lineation runs northwest from the north side of Newberry Caldera to Lava Butte and is very probably related to the Northwest Rift Zone described by Peterson et al. (1976).

A very distinct east-west lineation approximately 20 km long crosses the crest of the High Cascades at 43°40'N latitude. A recent geological map of the area by Peterson et al. (1976) shows no indication of any other faults or other lineations in the area. However, east of the crest of the High Cascades the anomaly aligns with Moore Creek, and west of the crest it aligns with the straight and flat east-west striking face of Mt. Ray, suggesting a possible unmapped fault.

LOW PASS FILTERED MAPS

Figures 7 and 8 show magnetic anomaly maps of the area which have been low-pass filtered to attenuate wavelengths shorter than 15 km and 25 km respectively. The spectrum of the entire data set (Figure 10) shows that the anomalies due to topography and shallow sources have wavelengths shorter than 15 km. However, many of the features that appear to be correlated with topography on Figure 5 also appear in Figure 7 (where wavelengths shorter than 15 km have been suppressed) suggesting that deeper sources are also present.

The northwest-southeast trends seen on the unfiltered magnetic anomaly map are also prominent in Figure 7, particularly in the southeast corner of the study area. More distinct however, are the north-south and north northwest-south southwest trends associated with the Basin and Range topography southeast of the study area. North-south trends appear in the Mt. Thielson-Mt. Bailey area and north of Newberry Crater. The north northeast-south southwest trends are visible from Walker Rim to Newberry and along the boundary between the Western Cascades and the High Cascades.

On Figure 8 (where wavelengths shorter than 25 km have been suppressed) most of the correlation between anomalies and topography has disappeared. The Three Sisters, Broken

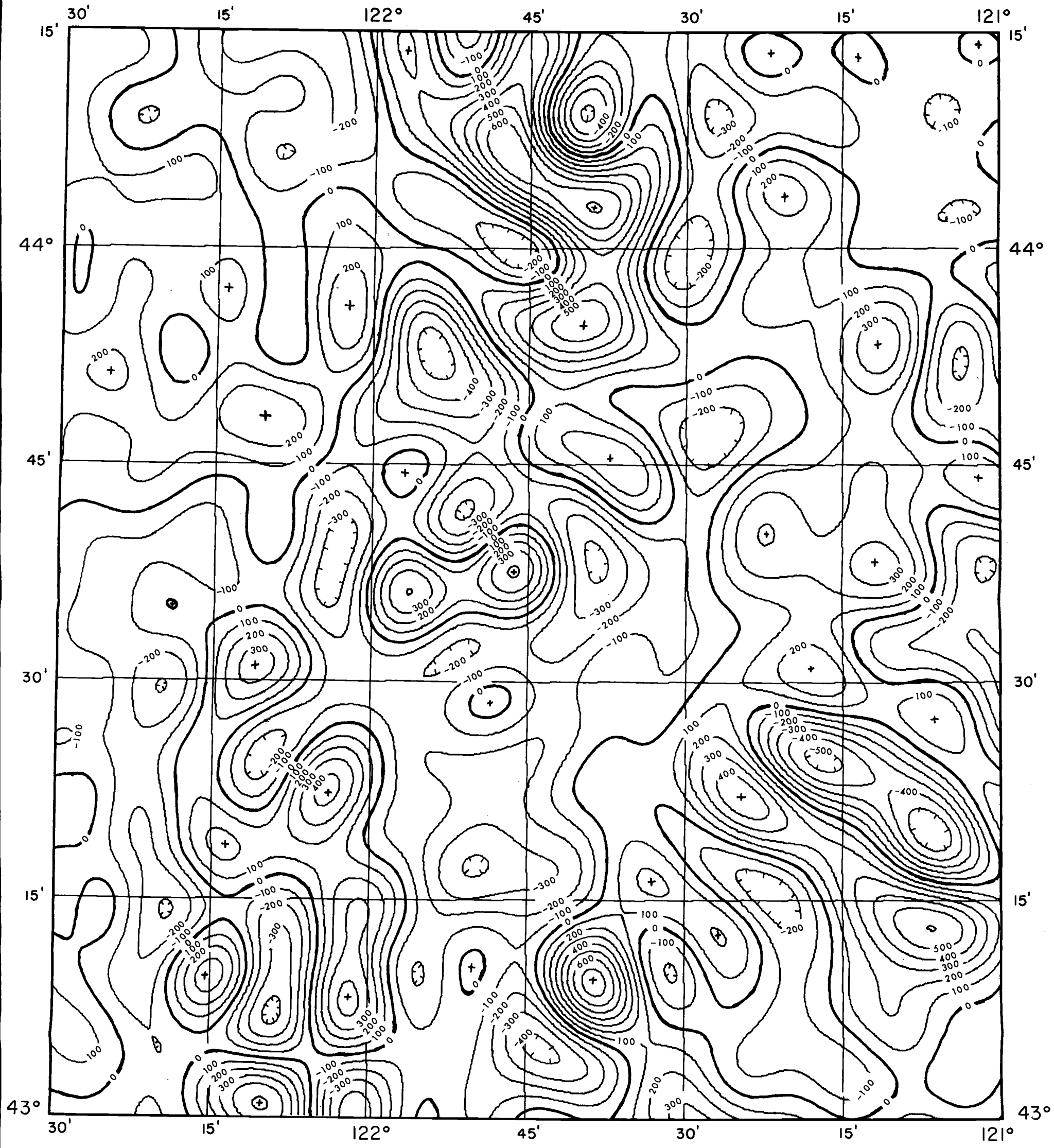

TOTAL FIELD AEROMAGNETIC ANOMALY MAP
LOW PASS FILTERED

CASCADE MOUNTAIN RANGE, CENTRAL OREGON

KILOMETERS
0 5 10 15 20
0 5 10
MILES

TOTAL FIELD DATA FROM:
GEOPHYSICS GROUP, OSU, 1977
I.G.R.F. 1975
DATA REFERENCE ELEVATION 9,000 FEET
CUTOFF WAVELENGTH 15 KM.

UNIVERSAL TRANSVERSE MERCATOR PROJECTION
CONTOUR INTERVAL 100 GAMMAS
ESTIMATED RMS UNCERTAINTY 4 GAMMAS
SCALE 1:500,000

OREGON STATE UNIVERSITY
AUGUST, 1979

FIGURE 7

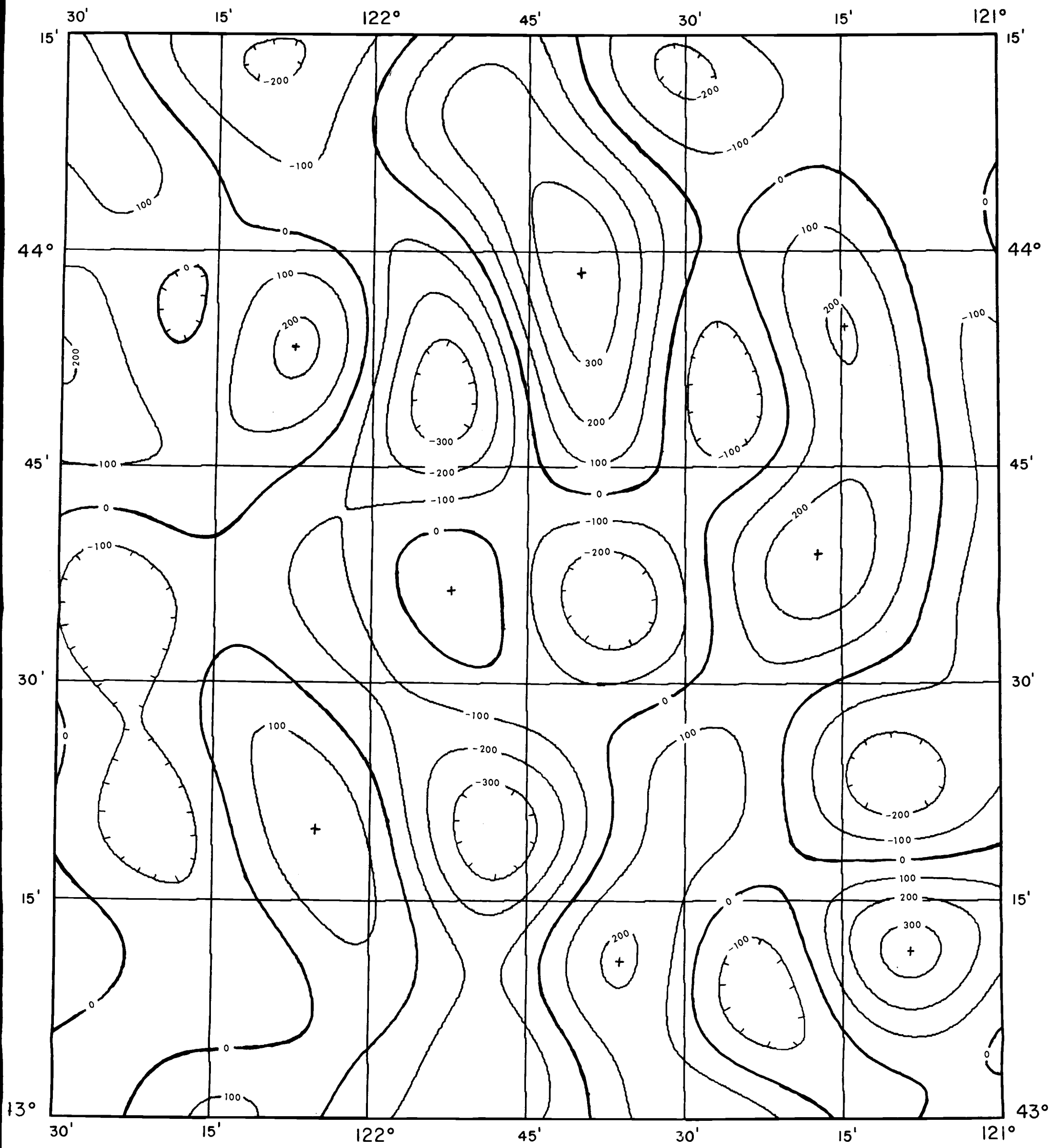

TOTAL FIELD AEROMAGNETIC ANOMALY MAP
LOW PASS FILTERED

CASCADE MOUNTAIN RANGE, CENTRAL OREGON

KILOMETERS
0 5 10 15 20
0 5 10
MILES

TOTAL FIELD DATA FROM:
GEOPHYSICS GROUP, OSU, 1977
I.G.R.F. 1975
DATA REFERENCE ELEVATION 9,000 FEET
CUTOFF WAVELENGTH 25 KM.

UNIVERSAL TRANSVERSE MERCATOR PROJECTION
CONTOUR INTERVAL 100 GAMMAS
ESTIMATED RMS UNCERTAINTY 4 GAMMAS
SCALE 1:500,000

OREGON STATE UNIVERSITY
AUGUST, 1979

FIGURE 8

Top, Batchelor Butte, and Lookout Mountain positive anomalies have merged to form a single large north-south feature, which suggests that they are related to some feature several kilometers deep.

In a detailed study of the Basin and Range faulting in Oregon, Donath (1962) identified two major fault trends, one about N 20° E to N 30° E and the other N 30° W to N 40° W. Lawrence (1976) recognized the same pattern over the entire area between the Brothers Fault zone and the Eugene-Denio zone. He found that most of the major basins and rim faults are related to the northeast-trending fault set. In the southeastern portion of Figure 8, this N 20° E to N 30° E trend has replaced the northwest-southeast trends seen in the other two maps containing shorter wavelength anomalies. A prominent pair of positive and negative anomalies strikes N 25° E from Walker Rim to Bend. The negative half of this pair of anomalies is located over the low terrain containing the Deschutes River and the La Pine Valley. Pitts (1979) also observed this same general trend in the gravity anomalies of this area. The magnetic and gravity anomalies suggest that this feature extends several kilometers deep in the crust and may indicate another basin structure here similar to the other Basin and Range structures to the southwest.

Because the declination of the geomagnetic field is approximately parallel to the structure (N 20° E) in

this area, the induced magnetic anomalies due to this structure will in general have lower amplitude than anomalies associated with other structural trends.

MAGNETIC SOURCE DEPTH DETERMINATIONS USING SPECTRAL ANALYSIS

Treitel et al. (1971) and Blakely and Hassanzadeh (1977) described one-dimensional approaches for calculating source depths from magnetic anomaly profiles which assume that the source bodies are infinite in the dimension perpendicular to the profile. However, Tsuboi and Fuchida (1937) have shown that the length of the source must be greater than six times the width for the error caused by the assumption of a linear source to be less than 10%. The length-to-width ratios of the anomalies of Figure 5 indicate that a two-dimensional approach is necessary for this area.

Gudmundsson (1978), Spector (1968), Naidu (1979), Spector and Grant (1970), Mishra and Naidu (1974), Bhattacharyya and Leu (1975) and Shuey et al. (1977) have described useful two-dimensional techniques for spectral analysis of aeromagnetic anomalies lacking linear features. Following Spector and Grant (1970) we assume that the anomalies on the aeromagnetic map are due to an ensemble of vertical sided prisms, hence the energy spectrum of the map in polar coordinates is:

$$\left\langle E(r,\theta)\right\rangle = 4\pi^2 M^2 R_G^2 \left\langle e^{-2hr}\right\rangle \left\langle (1-e^{-tr})^2\right\rangle \left\langle S^2(r,\theta)\right\rangle \left\langle R_p^2(\theta)\right\rangle \quad (1)$$

where $\langle\ \rangle$ indicates the expected value

M = magnetic moment/unit depth

h = depth to the top of the prism

t = thickness of the prism

S = factor for the horizontal size of the prism

R_p = factor for magnetization direction of the prism

R_G = factor for geomagnetic field direction.

Taking the average with respect to θ gives:

$$\left\langle \bar{E}(r) \right\rangle = 4\pi^2 M^2 R_G^2 \left\langle \bar{R}_p^2 \right\rangle \left\langle e^{-2hr} \right\rangle \left\langle (1-e^{-tr})^2 \right\rangle \left\langle \bar{S}^2(r) \right\rangle \qquad (2)$$

where $\bar{E}$, $\bar{R}$, $\bar{S}$ indicate the average over θ. Assuming that the distribution of the prism depths falls in the range $0.75\bar{h} < h < 1.25\bar{h}$ where $\bar{h}$ is the mean depth to the top of the prisms, Spector and Grant (1970) show that $\left\langle e^{-2hr} \right\rangle$ reduces to e^{-2hr} and have found from experience that it is the dominating influence on spectrum shapes. Figures 10 through 19 show plots of $\ln[E(r)/\bar{E}(0)]$, where $\bar{E}(0)$ is the energy of the zero frequency component of the anomalies.

The approach outlined above includes a number of additional assumptions:

(1) the anomaly field f(x,y) is the realization of a real, stationary, random process,

(2) the magnetization is zero except in discrete, uniformly magnetized bodies randomly located,

(3) the (x,y) coordinates of the body centers are statistically independent of the other body parameters, and

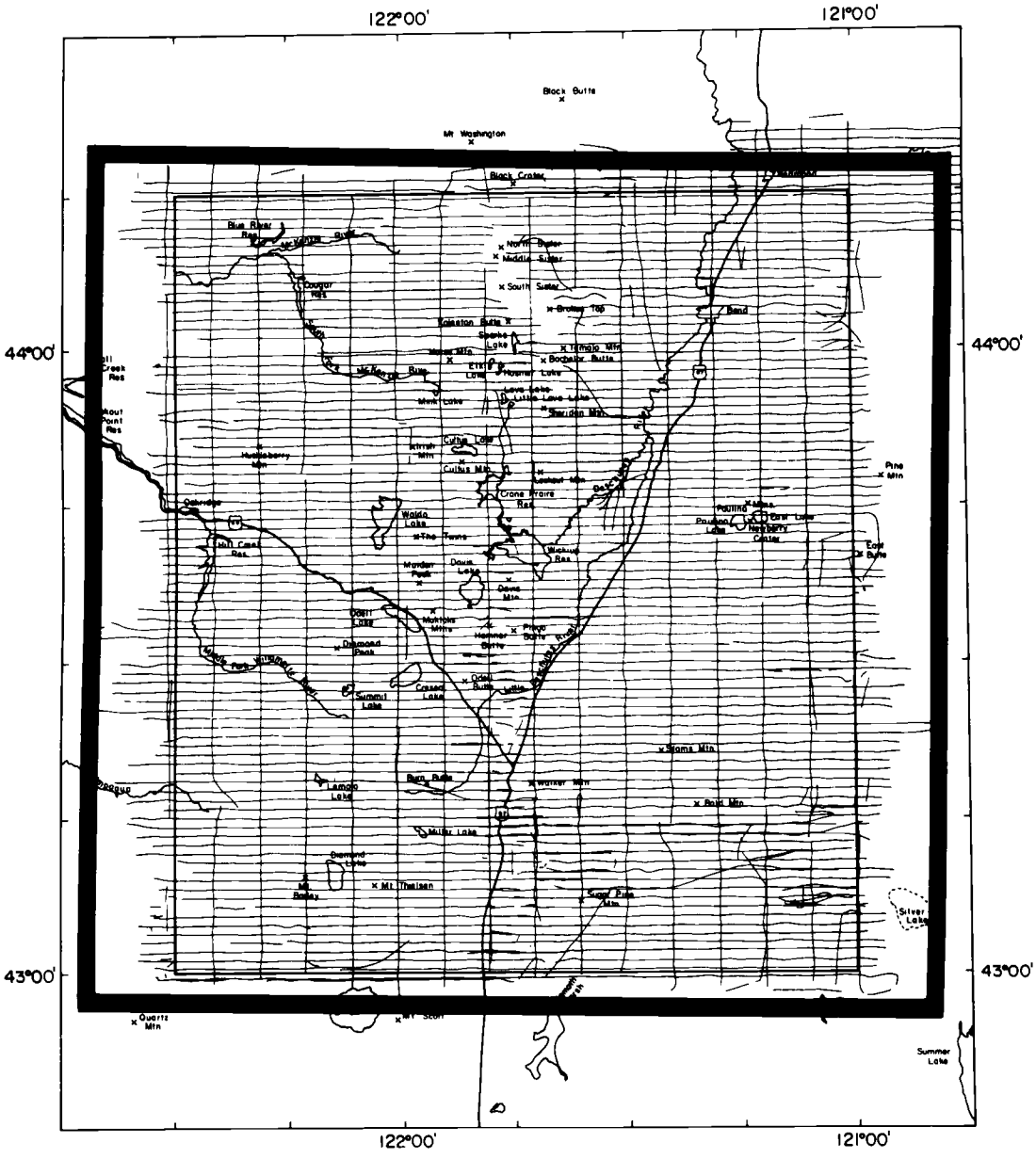

Figure 9. Boundaries of 512 x 512 grid. Heavy black lines show the boundaries of 512 x 512 grid. Values at the boundary are set to zero.

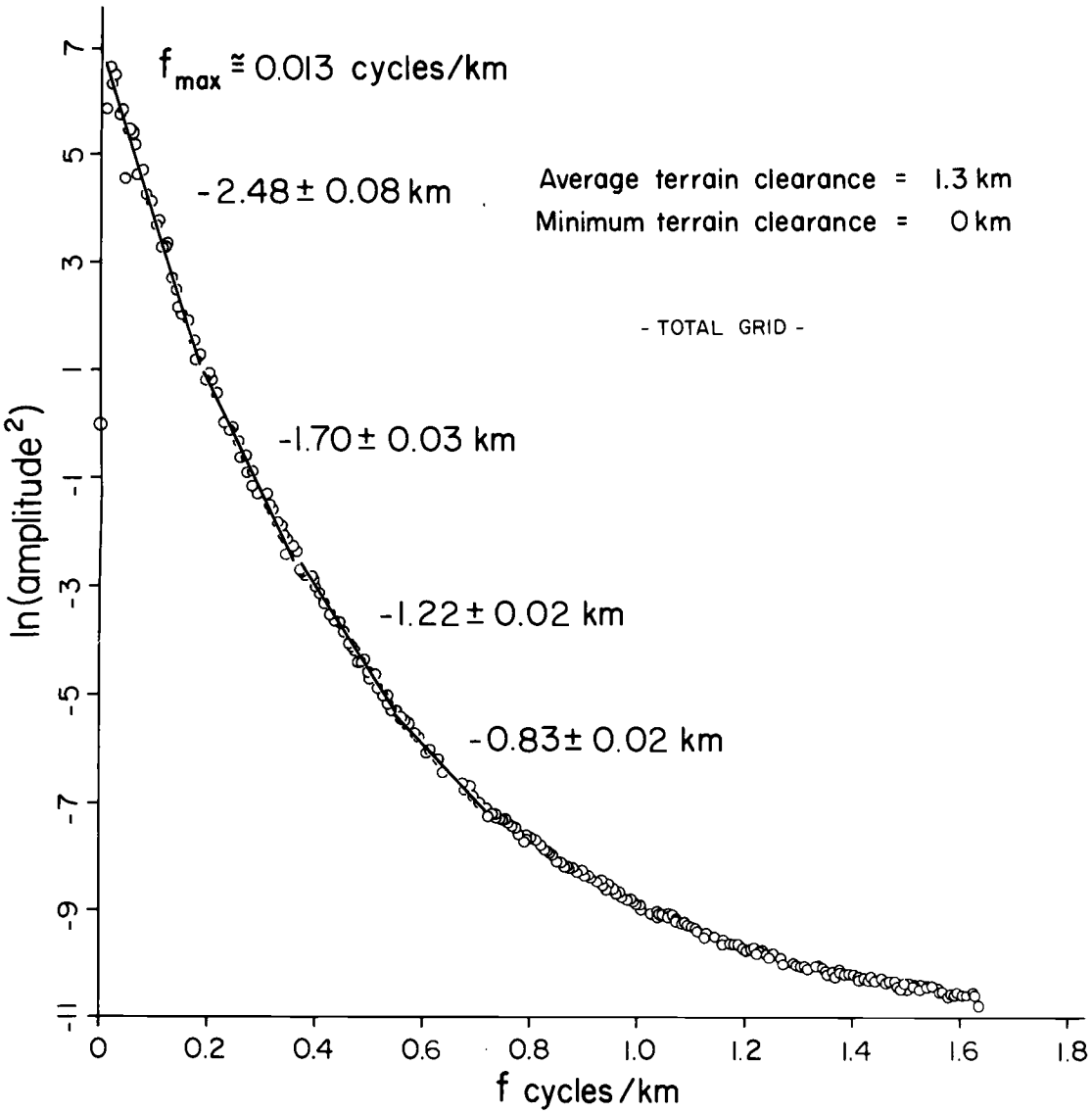

Figure 10. Radially averaged spectrum of the Central Oregon Cascades aeromagnetic data.

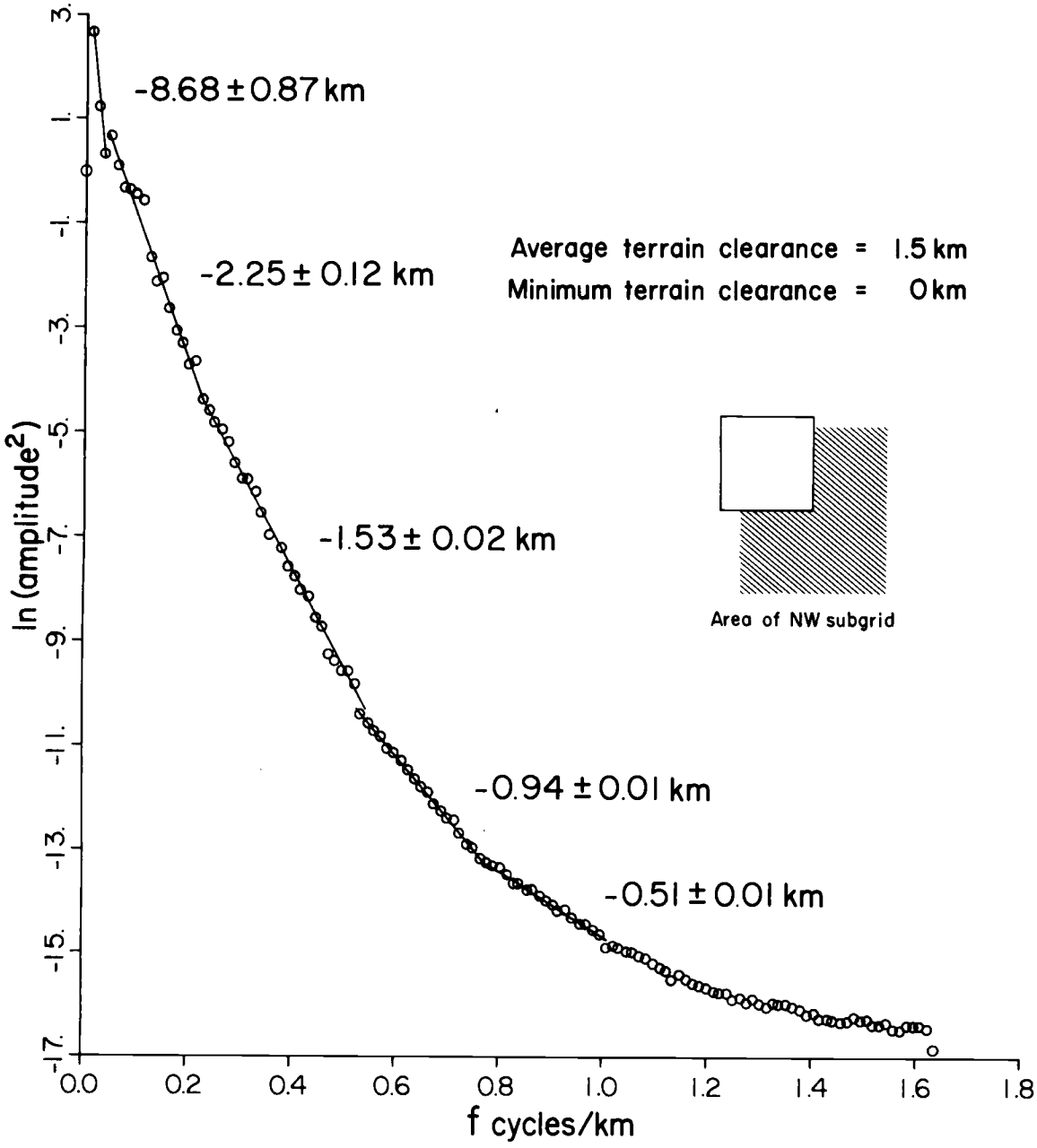

Figure 11. Radially averaged spectrum of the north-west portion of the Central Oregon Cascades aeromagnetic data.

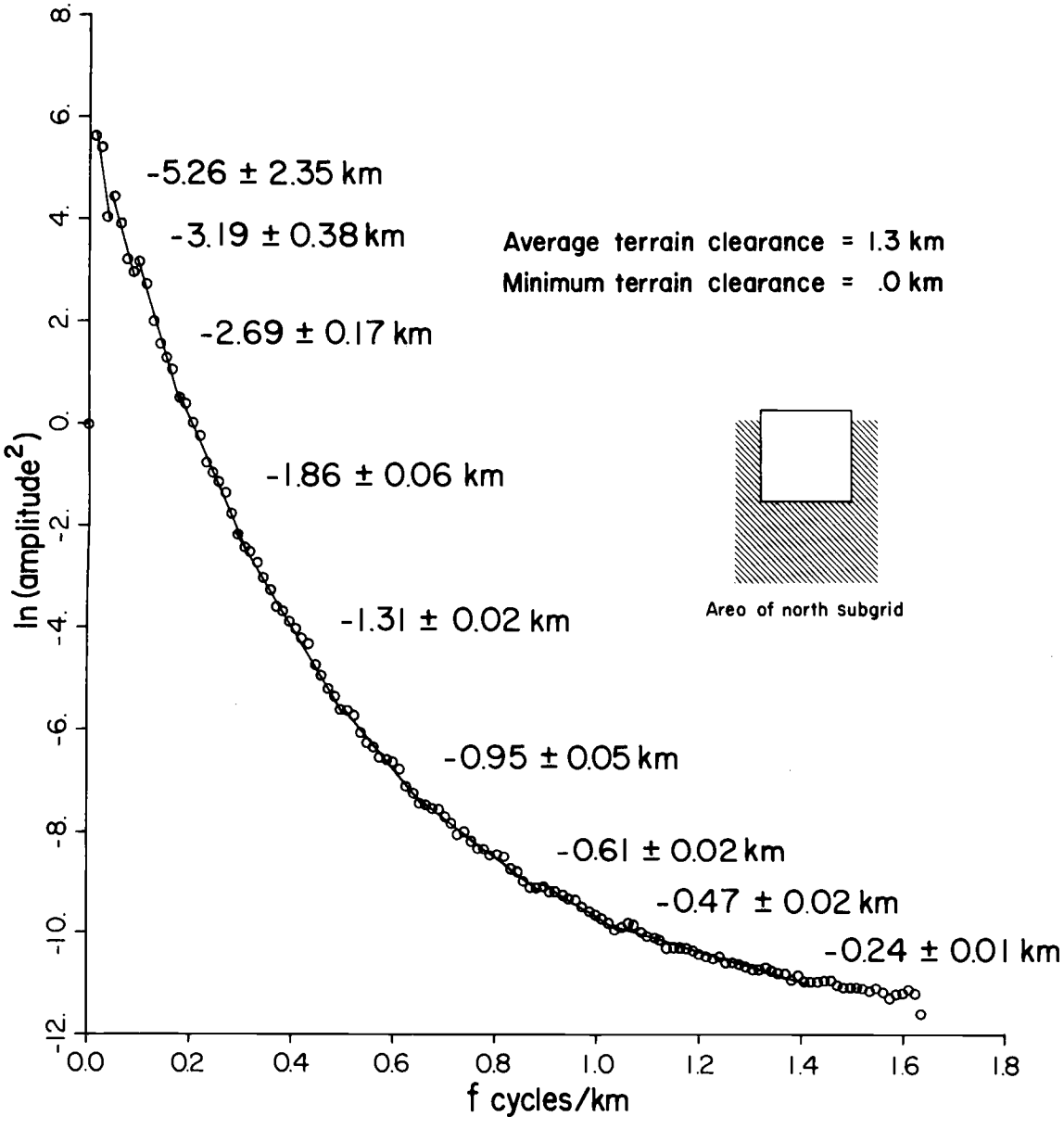

Figure 12. Radially averaged spectrum of the north portion of the Central Oregon Cascades aeromagnetic data.

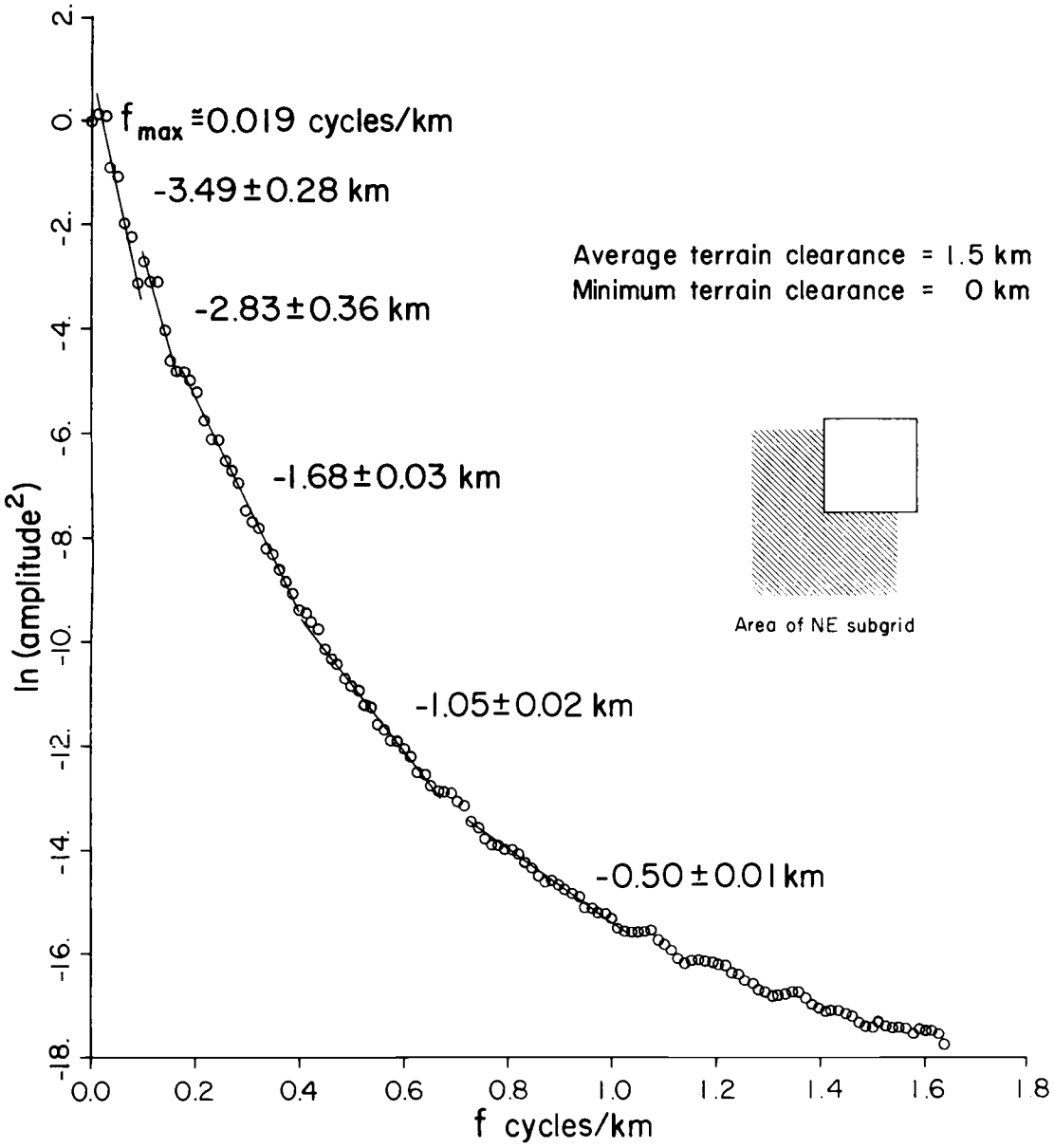

Figure 13. Radially averaged spectrum of the north-east portion of the Central Oregon Cascades aeromagnetic data.

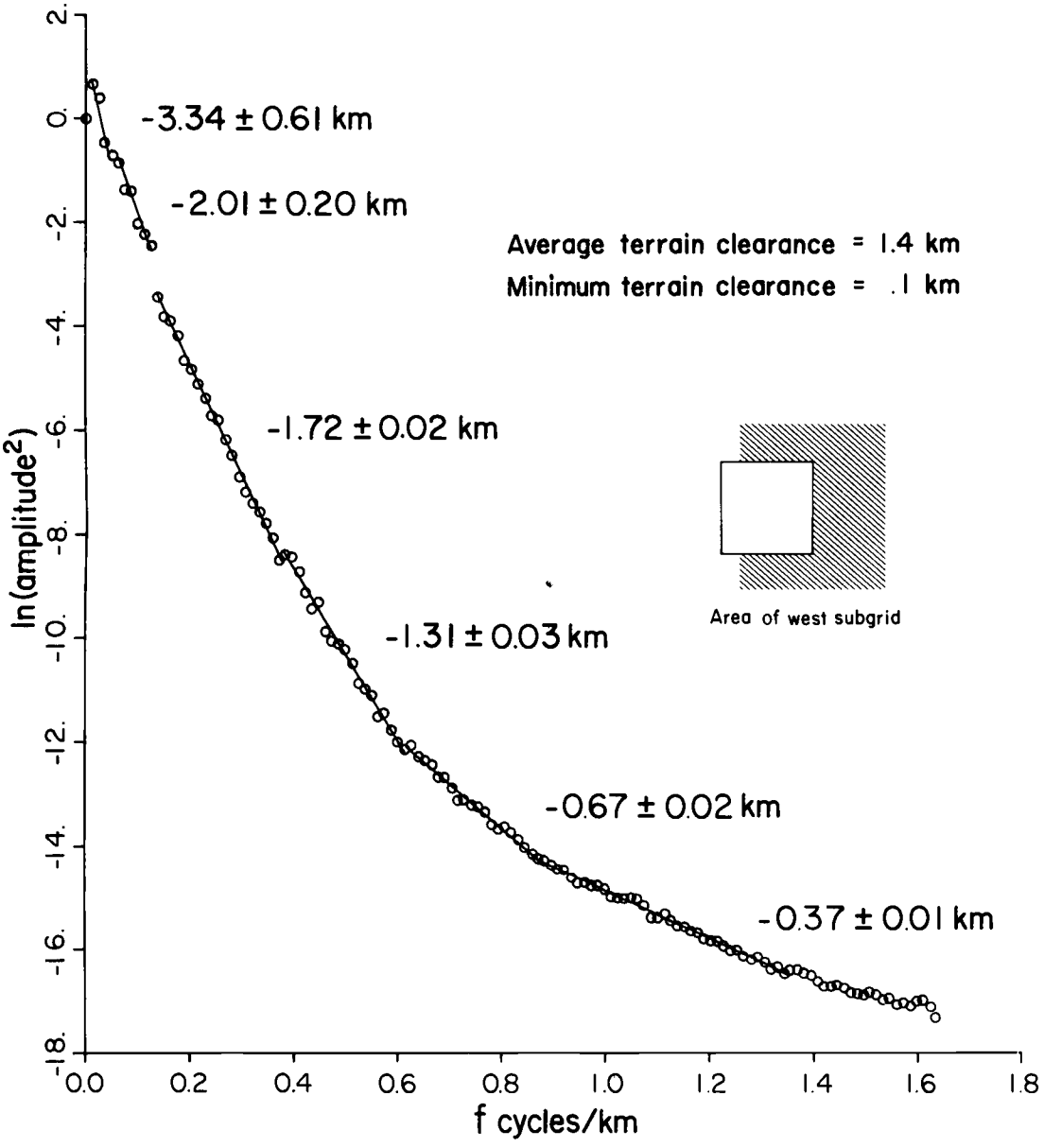

Figure 14. Radially averaged spectrum of the west portion of the Central Oregon Cascades aeromagnetic data.

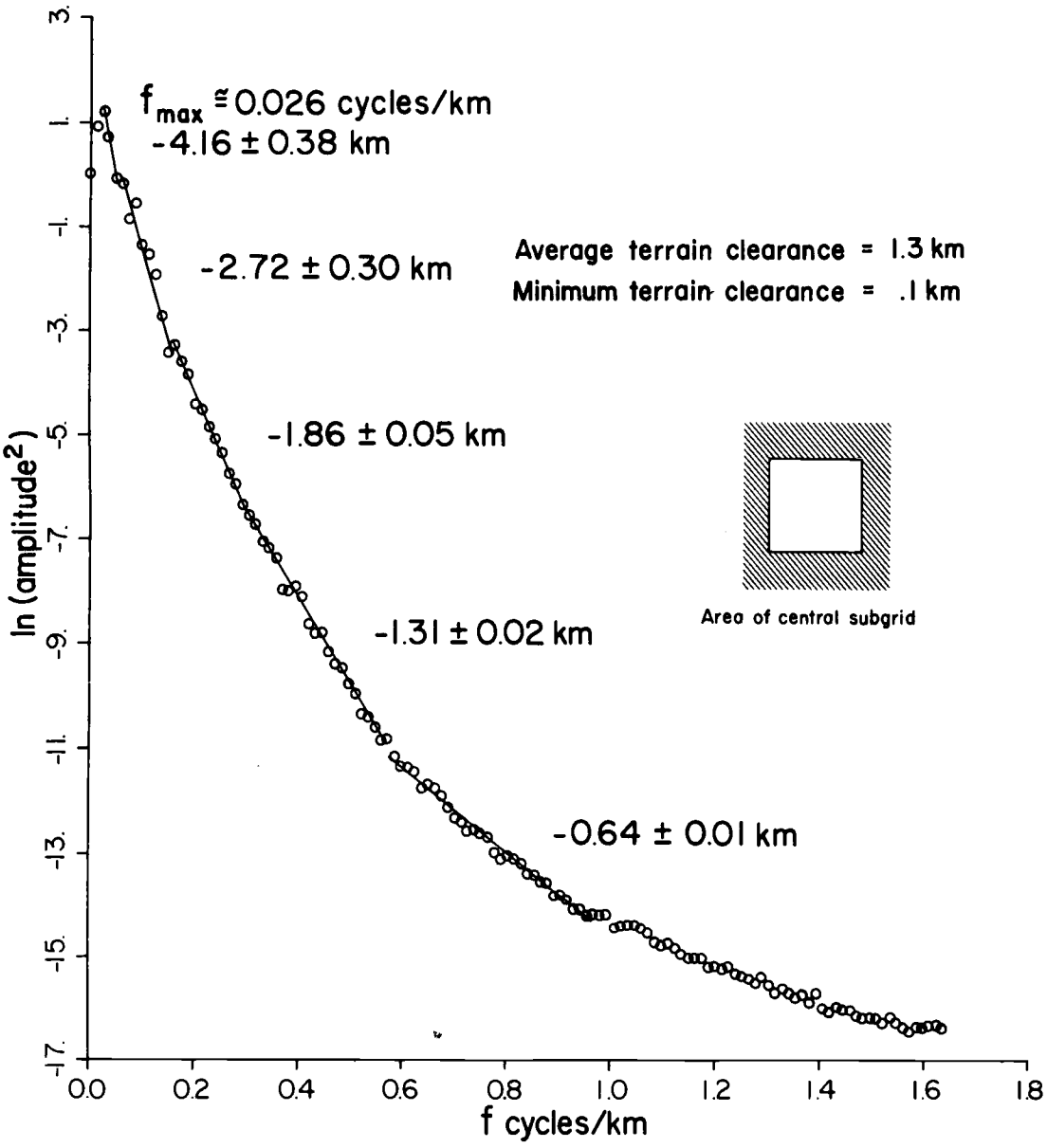

Figure 15. Radially averaged spectrum of the center portion of the Central Oregon Cascades aeromagnetic data.

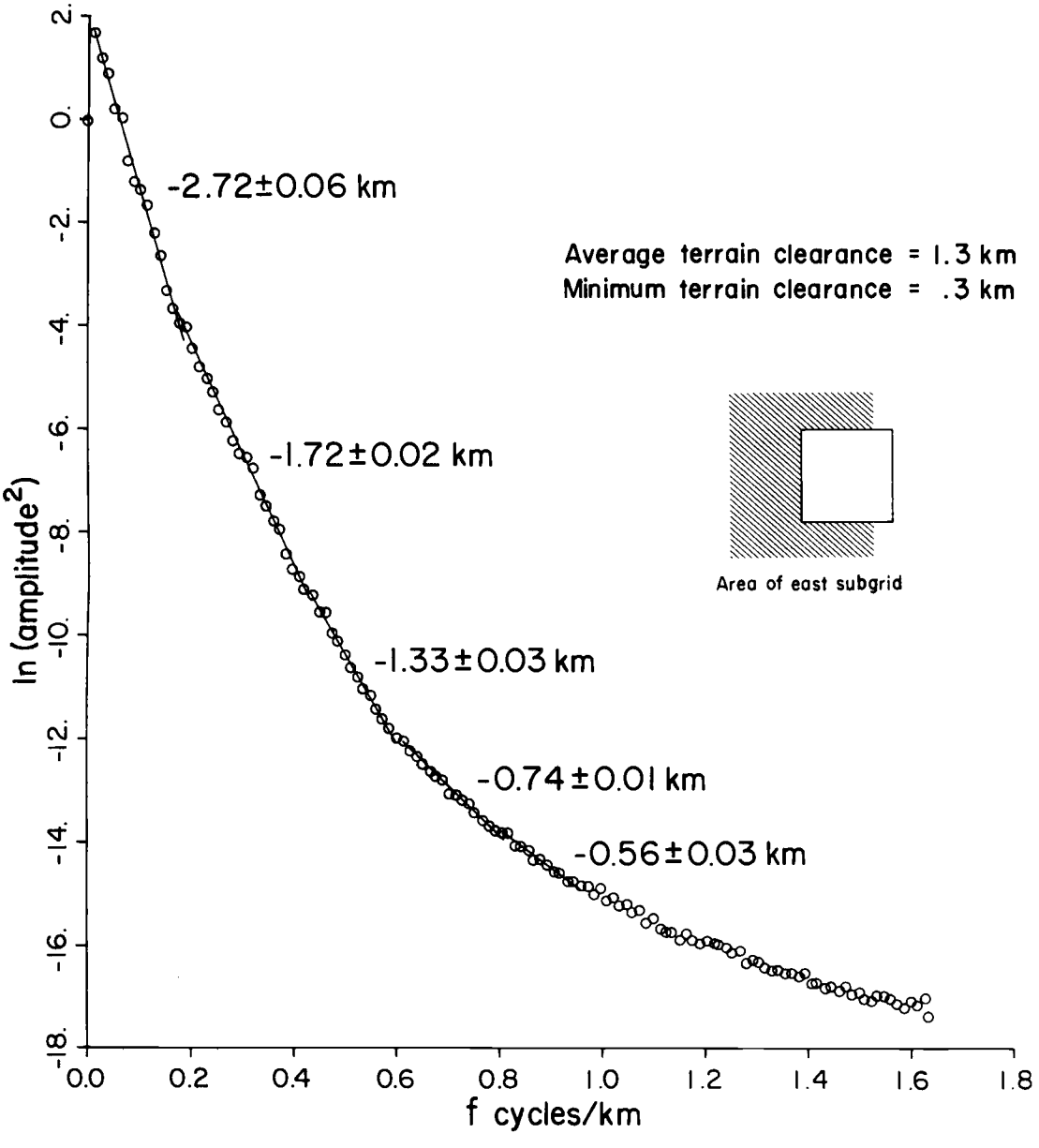

Figure 16. Radially averaged spectrum of the east portion of the Central Oregon Cascades aeromagnetic data.

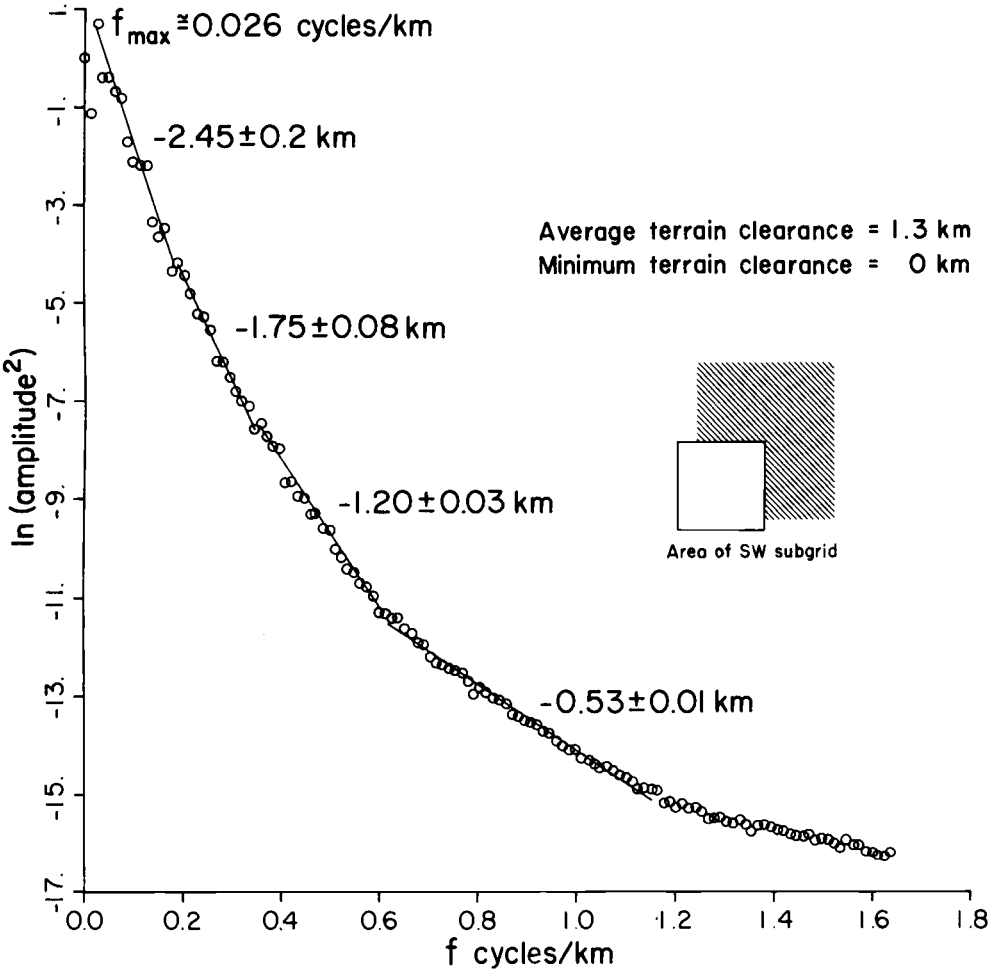

Figure 17. Radially averaged spectrum of the south-west portion of the Central Oregon Cascades aeromagnetic data.

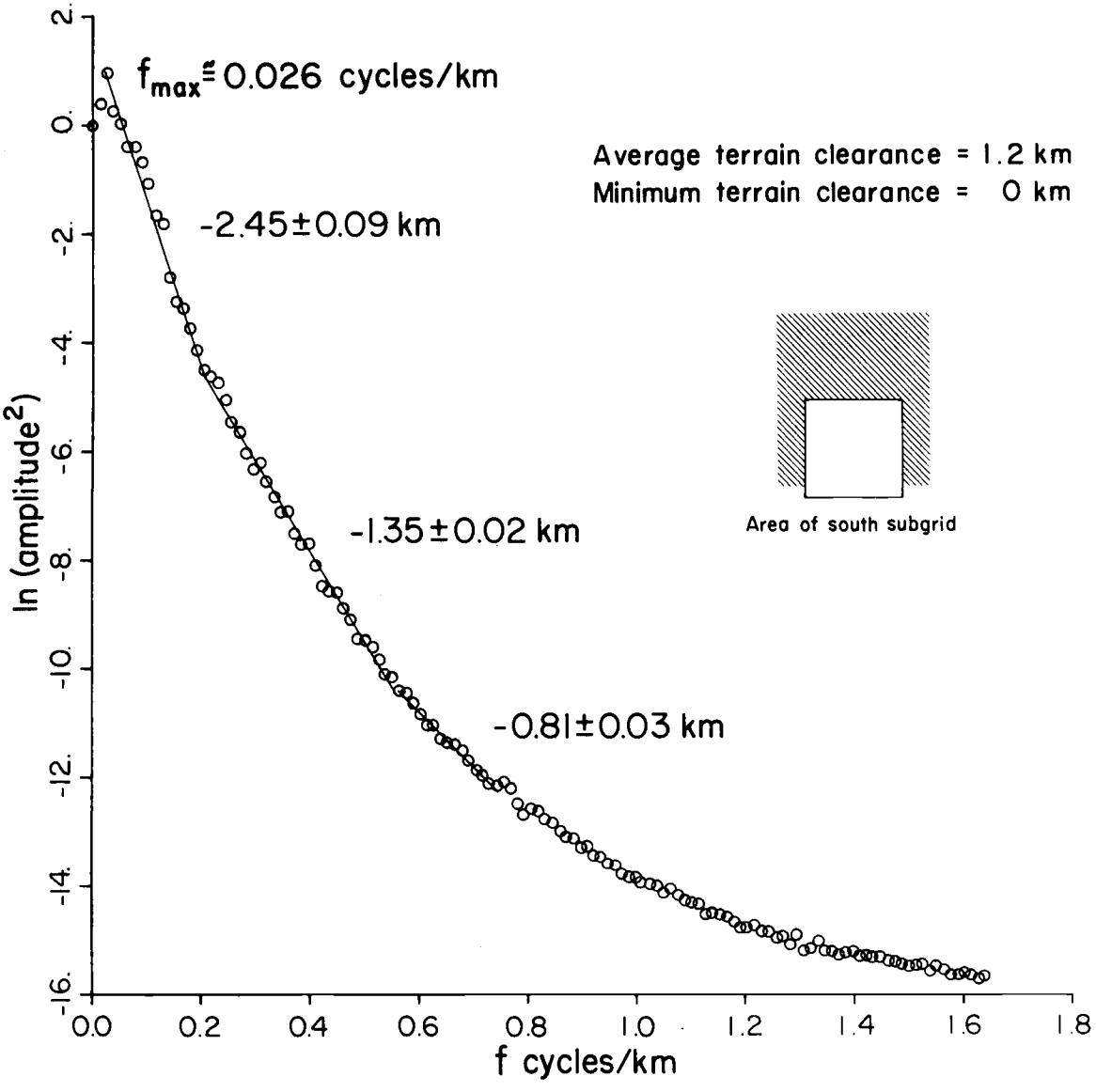

Figure 18. Radially averaged spectrum of the south portion of the Central Oregon Cascades aeromagnetic data.

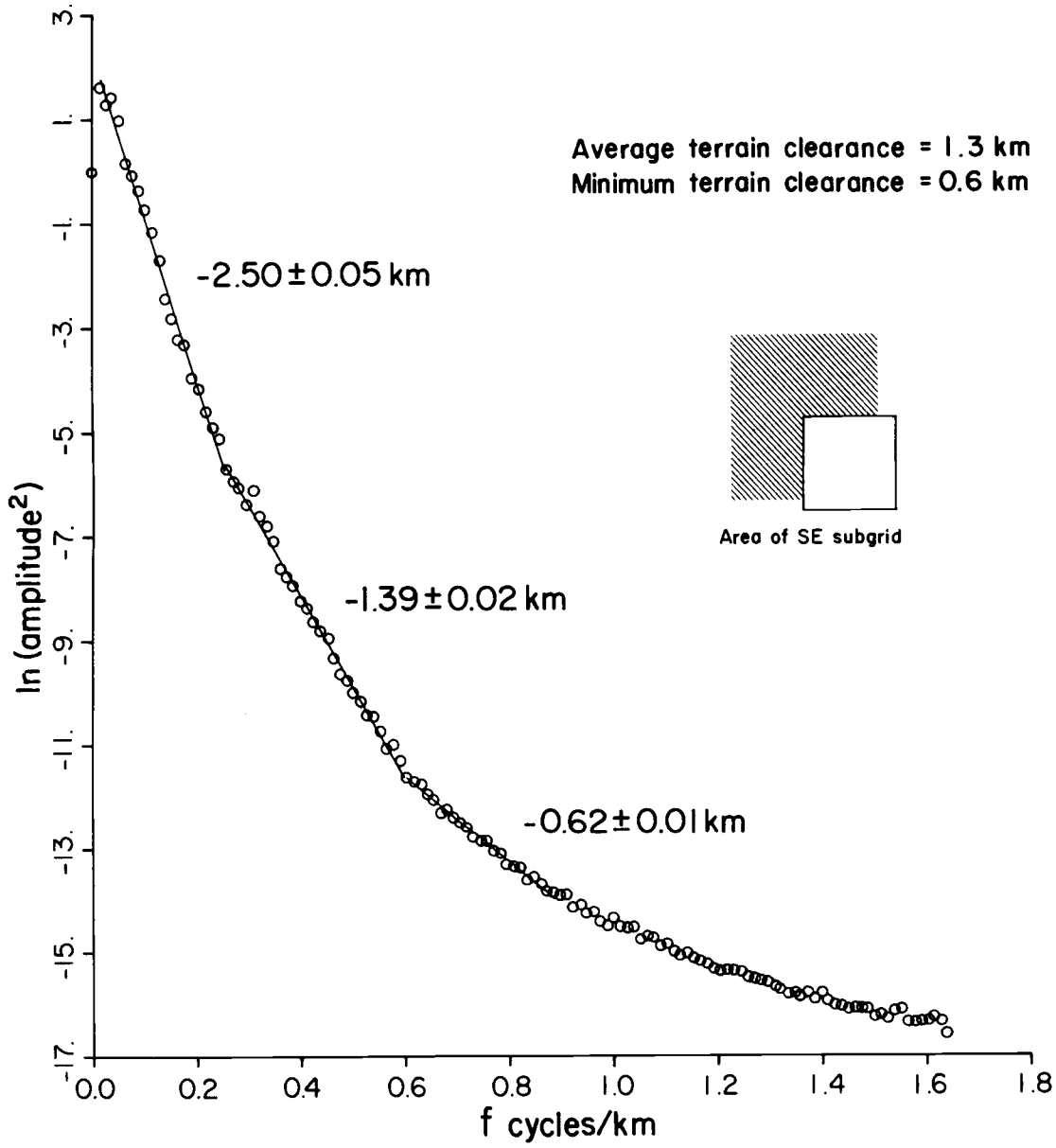

Figure 19. Radially averaged spectrum of the south-east portion of the Central Oregon Cascades aeromagnetic data.

(4) the magnetization direction is approximately parallel to the geomagnetic field direction (within ±20°).

All the measurements collected at a flight elevation of 2.74 km, including data from just outside of the survey area as shown in Figure 9, were used to create a uniformly spaced 512 x 512 point grid. Figure 10 represents the spectrum of the anomaly field, shown in Figure 5, computed from the entire 512 x 512 point grid. A series of nine overlapping 256 x 256 subgrids were extracted from the main grid. Figures 11-19 represent the spectrum of the nine 256 x 256 subgrids. The nine subgrids each cover one-fourth of the total grid. The subgrids were overlapped in an attempt to increase resolution while retaining the capacity to discern deeper sources than would be possible with smaller grids.

The intervals of the least-squares, best fit straight lines drawn on the spectra, were chosen to minimize the standard deviation of the slope of the lines. The points at the high frequency end of the spectrum result from noise and from sources close to the flight level. The numbers beside the straight lines are the source depths and standard deviations calculated from the slope of the lines (see Appendix C). The indicated average terrain clearances were estimated from the 1:250,000 U.S.G.S. topographic maps of the area. The indicated minimum terrain clearances

reflect the highest terrain in the grid area. For some grids the terrain actually extended above the flight elevation between flight lines resulting in a zero minimum terrain clearance.

The spectrum of the entire area shown in Figure 10 appears much smoother than the spectra of the subgrids and does not show clearly discernable changes in slope. This probably results from the four distinct geologic-physiographic provinces included in the area which smear the distribution of source depths, especially for shallow sources. In fact, Naidu (1970) suggests that assumption (1) listed above is only reasonable for surveys restricted to one geologic province.

Table 3 summarizes the source depth information obtained from each spectrum. All the spectra show shallow source depths within 0.2 km of the estimated mean terrain level.

Because each 256 x 256 subgrid shares 50% of its data with adjacent grids, many of the source depths are similar between neighboring grids. For example, the deepest sources listed for the south and southeast areas probably result from the same sources. Both lack any detectable intermediate sources. Similarly, the intermediate source depths appear continuous between the northeast and east grids at approximately 1.0 km ASL, between the north and center grids at sea level and approximately 0.9 km ASL, and

Grid Location	Mean Terrain Clearance of Survey km (estimated)	Mean Elevation of Terrain km ASL (estimated)	Source Depths km from sea level (-below, +above)			
			Deep	Intermediate		Shallow
Total (512 grid) 43°00'-44°15' N lat. 121°00'-122°30' W long.	1.3	1.4		+0.26±.08	+1.04±.03	+1.52±.03
NW (256 grid) 43°38'-44°15' N lat. 121°45'-122°30' W long.	1.5	1.2	-5.94±.87	+0.49±.12		+1.21±.02
North (256 grid) 43°38'-44°15' N lat. 121°22'-122°08' W long.	1.3	1.4	-2.52±2.35 ---------- -0.45±.38	+0.05±.17	+0.88±.06	+1.41±.02
NE (256 grid) 43°38'-43°15' N lat. 121°00'-122°45' W long.	1.5	1.2	-0.75±.28	+0.09±.36	+1.06±.03	+1.69±.02
West (256 grid) 43°18'-43°57' N lat. 121°45'-122°30' W long.	1.4	1.3	-0.60±.61	+0.73±.20	+1.02±.02	+1.43±.03
Center (256 grid) 43°18'-43°57' N lat. 121°22'-122°08' W long.	1.3	1.4	-1.42±.38	+0.01±.03	+0.88±.05	+1.43±.02
East (256 grid) 43°18'-43°57' N lat. 121°45'-121°45 W long.	1.3	1.4		+0.01±.06	+1.02±.02	+1.41±.03
SW (256 grid) 43°00'-43°38' N lat. 121°45°-122°30' W long.	1.3	1.4		+0.29±.20	+0.99±.08	+1.54±.03
South (256 grid) 43°00'-43°38' N lat. 121°22'-121°08' W long.	1.2	1.5		+0.29±.09		+1.43±.02
SE (256 grid) 43°00'-43°38' N lat. 121°00'-121°45' W long.	1.3	1.4		+0.24±.05		+1.35±.02

Table 3. Source depths from spectral analysis of aeromagnetic anomalies.

and between the west and southwest grids at approximately 1.0 km ASL. The southwest and south spectra also show the same deep source depths at approximately 0.29 km ASL. The long wavelength portion of the northwest spectrum is very different from the other spectra. It contains the highest percentage of information from the Western Cascades province, which may explain the significantly deeper source depth of approximately 6 km BSL.

For 7 of the 10 grids, all of the source depths were less than 3.5 km below survey level. Grids of this size (77 km) should be able to see sources as deep as 12 km. It is possible that these shallow source depths are artifacts of the processing technique. However, the same technique used on a very similar aeromagnetic survey in eastern Oregon (Boler, 1978) yielded a very different set of source depths. Using smaller grids, Boler (1978) found sources deeper than 3.5 km below the survey level for five out of six grids. The extensive amount of volcanism in this area suggests another explanation. The deeper crust is no longer likely to appear as distinct layers with significant contrasts of magnetization. Igneous sills, dikes, and plutons may be so numerous that any weakly magnetic layers are no longer visible. Wasilweski et al. (1979) point out that with increasing depth and temperature viscous magnetization is enhanced and the remanent component is diminished. The deeper a magnetic rock is

within the crust, the greater is the component of magnetization along the present geomagnetic field. This effect is enhanced in areas with high thermal gradients such as the Central Cascades area.

The geological and physiographic complexity of this study area also complicates the interpretation of source depths. Most of the grid areas contain significant parts of more than one geologic province. The low frequency portion of all the spectra except the southeast and east grids show unexpected roughness. This effect may be due to the presence of a relatively small number of source bodies, with large horizontal dimensions, in the upper crust. The statistical nature of the computational model used here requires the sources to fall into distinct ensembles with ensemble average depths $\bar{h}$ for the range of depths $\bar{h} \pm \Delta h$ such that $\Delta\bar{h}/h < .25$. The extensive evidence of young volcanism suggests that this area may violate this assumption of the computational model.

CURIE ISOTHERM DEPTH DETERMINATIONS FROM SPECTRAL ANALYSIS

Estimates of the thickness of the magnetized portion of the earth's crust suggest that there are two types of lower boundaries of the layer of magnetized rocks. One type of boundary corresponds to vertical changes in composition within the crust. In areas characterized by normal and low heat flow such as the Siberian (Bulina, 1961), the Canadian (Hall, 1968), and the Brazillian (Gasparini et al., 1979) continental shields, the bottom of bodies causing regional magnetic anomalies seem to coincide with an intracrustal seismic discontinuity suggesting a lithologic interface.

The second type of boundary occurs where high temperatures at depth cause the rocks to lose their ferromagnetic properties (the Curie point isotherm depth). The relatively young age of the crust and the high heat flow of this study area suggests the second type of boundary. The Cenozoic volcanic features present over most of the area imply a large number of intrusive bodies extending well below the computed source bottoms, perhaps to the base of the seismic crust.

With increased interest in geothermal resources, investigators have used several techniques to determine the Curie point isotherm depth, with varying degrees of success.

Bhattachartta and Morley (1965) analyzed individual anomalies assumed to be caused by intrusive bodies which could be modeled by vertical-sided prisms. The horizontal dimensions and depth to top were determined by graphical means. They then used the first vertical derivative and amplitude of the anomaly to obtain the magnetization and Curie point depth of each anomaly.

In an analysis of aeromagnetic data from Yellowstone Park, Bhattacharyya and Leu (1975) used a combination of isolated anomaly analysis and operations on the Fourier transform of anomalies within 31 km x 31 km blocks to look for variations in the Curie point isotherm depth. Byerly and Stolt (1977) compared the spectrum of individual anomalies from an aeromagnetic survey of the State of Arizona with the spectrum of a model vertical prism or cylinder.

Shuey et al. (1977) also attempted to determine Curie depth by analysis of individual anomalies but concluded that the task was impossible with their data set. Assuming a bottomless prism, they obtained a fit not significantly worse than the best fit obtainable with any prism model. Shuey et al. (1977) and Boler (1978) also point out the difficulty of finding anomalies which are isolated enough so that adjacent anomalies do not overlap. Because the average value of the anomaly due to a depth-limited prism or cylinder is zero, it has a negative part as well as a

positive part. Assuming normal magnetization, the positive part of the anomaly contains information about the horizontal dimensions and the depth to the top of the source. The negative part, which contains most of the information about the bottom of the source, is of relatively low amplitude and spread over a large area. However, the negative parts of the anomalies are included in the power spectrum and their relative contribution is larger at longer wavelengths which suggests that spectral analysis may be a better approach.

This study uses the same method as Smith et al. (1974) and Boler (1978). They used the effect of the factor $(1-e^{-tr})^2$ in equation (2) to find the thickness of the deepest magnetic layer. If the map is large enough so that the low frequency anomalies caused by the bottom of sources are included in the anomaly map, the factor $(1-e^{-tr})^2$ in combination with the factor e^{-2hr} introduces a peak or maximum in the spectrum, related to the depth of the bottom of the source (Spector and Grant, 1970). The longest wavelength for which the Fourier transform can be calculated is the total length of the map. The spectrum of the map only contains depth information down to a depth of length/2π (Shuey et al., 1977). If the source bodies have bottoms deeper than $L/2\pi$, the spectral peak occurs at a frequency lower than the fundamental frequency for the map and cannot be resolved by spectral analysis.

The horizontal dimensions of the source bodies also affect the predicted spectrum and the appearance of the spectral peak. For a body of infinite horizontal extent, the peak is displaced to zero frequency and does not appear in the spectrum regardless of the depth of the source bottom. For finite size maps a source body will appear infinite if its dimensions are comparable to the map area. Shuey et al. (1977) point out that such a body would simulate a regional gradient of magnetization, so the magnetic anomaly field f(x,y) could not be considered a realization of a stationary, random process. In this study the regional trend in the Central Cascades data was removed by subtracting the value of a plane fit to the gridded data by the method of least-squares. The expression for the plane is

$$f(x,y) = 25.25 - .89x + .39y \quad \text{(gamma)}$$

where x is positive, y is positive north and x and y are the distances in kilometers from the southwest corner of the grid. This detrending process forces the amplitude of the zero frequency component E(0) lower than the fundamental frequency E(1) so that all of the spectra shown in Figures 10-19 show at least a one point spectral peak. However only those spectra exhibiting more than a one point peak were used in this study to estimate Curie point depths.

When a significant spectral maximum does occur, indicating that the source bottoms are detectable, the frequency of the spectral peak (f_{max}), the mean depth to the source tops (h), and the mean depth to the source bottom (d) are related by

$$f_{max} = \frac{1}{2\pi(d-h)} \ln \frac{h}{d} .$$

The spectrum of the main grid (Figure 10) and the spectrum of four of the nine subgrids, southwest (Figure 17), south (Figure 18), center (Figure 15), and northeast (Figure 13) show two point spectral peaks. The frequency of the spectral maximum ranges from .013 to .026 cycles/km. Researchers working in other parts of the western U.S. have observed spectral peaks in this same general range (Shuey et al., 1977; and Boler, 1978).

Table 4 gives Curie point isotherm depths estimated from the frequency of the spectral maximum. The corresponding geothermal gradients and surface heat flow values are based on possible Curie point temperatures of 300°C and 580°C using a conductivity of 2.5 $Wm^{-1}°C^{-1}$, given by Stacey (1977) as the average for igneous rocks.

The average surface heat flow for the study area is given by Blackwell et al. (1978) as 100 mW/m^2 although the 15 individual measurements made in their study range from less than 20 to greater than 120 mW/m^2, with vertical gradients as high as 78°C/km. Their heat flow map of

Grid location	Total (512 grid) 43°00'-44°15' N lat. 121°00'-122°30' W long.		SW (256 grid) 43°00'-43°38' N lat. 121°45'-122°30' W long.		South (256 grid) 43°00'-43°38' N lat. 121°22'-122°08' W long.		Center (256 grid) 43°18'-43°57' N lat. 121°22'-122°08' W long.		NE (256 grid) 43°38'-44°15' N lat. 121°00'-121°45' W long	
Sized grid	155 km x 155 km		77 km x 77 km		77 km x 77 km		77 km x 77 km		77 km x 77 km	
Mean terrain elevation ASL	1.4		1.4		1.5		1.4		1.2	
Frequency of the spectral peak f_{max}	.013		.026		.026		.026		.019	
	MINIMUM CURIE DEPTHS - (5 km thick sources)									
Curie depth km below survey level	15		9		9		9		11	
km BSL	12		6		6		6		8	
	T_C=580°C	T_C=300°C	T_C=580°C	T_C=300°C	T_C=580°C	T_C=300°C	T_C=580°C	T_C=300°C	T_C=580°C	T_C=300°C
Vertical temp gradient °C/km	42	21	76	38	75	38	76	38	61	30
Surface heat flow *mW/m^2	105	53	190	95	188	95	190(71)	95	153	75
	MAXIMUM CURIE DEPTH									
Depth below survey level to top of source (km)	4.5		2.5		2.5		4.5		3.5	
Curie depth km below survey level	28		12		12		10		17	
km BSL	25		9		9		7		14	
	T_C=580°C	T_C=300°C	T_C=580°C	T_C=300°C	T_C=580°C	T_C=300°C	T_C=580°C	T_C=300°C	T_C=580°C	T_C=300°C
Vertical temp gradient °C/km	21	11	54	27	53	27	67	33	37	18
Surface heat flow* mW/m^2	53	27	135	67	133	67	167(63)	83	92	46

* Heat flow based on a conductivety k = 2.5 $Wm^{-1}{}^{\circ}C^{-1}$ except ( ) which is based on k = .94 $Wm^{-1}{}^{\circ}C^{-1}$

Table 4 Curie point isotherm depths from spectral analysis of aeromagnetic anomalies, and corresponding surface heat flow and temperature gradients.

Oregon shows a steep gradient along the boundary between the Western Cascades and the High Cascades with the local maximum over the center of the study area. Blackwell et al. (1978) also state that rocks in the southeastern part of Oregon have an average thermal conductivity of 1.1 $Wm^{-1}°C^{-1}$. They use 0.94 $Wm^{-1}°C^{-1}$ as the conductivity of the basin fill in their thermal model of the Basin and Range province in Oregon. If their value for the conductivity of basin fill is used to recalculate the surface heat flow value for the center grid, the result is 63 to 71 mW/m^2, which is lower than the area average and may explain the low values shown in the La Pine Valley on their map.

The minimum Curie point depths shown in Table 4 were estimated by assuming a source thickness of 5 km. Assuming a thinner source would yield a shallower Curie point depth but requires unreasonably large values for source body magnetization. The maximum Curie point depths were estimated using the deepest source calculated from the slope of each subgrid using equation (2). The deepest source depth in the center grid provided the "h" for the main grid.

The significantly deeper Curie point depth calculated for the total grid represents an average value for the entire study area including the subgrids where spectral maxima did not occur. However, the heat flow calculations indicate that the maximum Curie point depth calculated for the entire area is probably too deep. In fact the heat

flow data suggests that all of the subgrids except the northwest and west grids should be able to "see" down to the Curie point depth. Shuey et al. (1977) pointed out that wide source bodies will steepen the spectrum and move the spectral peak to lower frequencies, thereby eliminating the peak altogether for sources where horizontal dimensions are on the order of the map size divided by 2π or 12 km for a 256 x 256 grid (77 km x 77 km). It is possible that the broad Paulina shield associated with Newberry Crater in the east, the Stams Mountain volcanics in the southwest, and Three Sisters complex in the north are underlain by coherent source bodies large enough to eliminate the spectral peak for the east, the southwest and the north subgrids, respectively.

A standard assumption in Curie point depth analysis is a Curie temperature of approximately 580°C, which is the Curie point temperature of magnetite (Fe_3O_4)(Bhattacharyya and Leu, 1975; Shuey et al., 1977). However, Haggerty (1978) cautioned against assuming a single Curie point temperature for continental crust and pointed out that Curie point temperatures as low as 300°C may exist in the crust because of the low temperature oxidation of titanomagnetite. Table 4, therefore, gives the heat flow and thermal gradients calculated for Curie point temperatures of both 580°C and 300°C. If the thermal gradient and heat flow values for the area given by Blackwell et al. (1978)

are representative, the Curie point temperatures appear to be closer to 580°C than to 300°C or the Curie point depths are shallower than calculated here.

STRUCTURAL IMPLICATIONS OF AEROMAGNETIC ANOMALIES AND INTERPRETATION OF CURIE POINT DEPTHS

Figure 20 summarizes the regional structural and subsurface thermal interpretations of the Central Cascades aeromagnetic anomaly data. The Eugene-Denio lineations (labeled ED on the figure), the Brothers fault zone (labeled B), and the Sisters fault zone (labeled S) are after Lawrence (1976) and correlate well with trends seen in the unfiltered and low-pass filtered magnetic anomaly maps. The very prominent broad negative anomaly in the Fort Rock Valley suggests a normal fault labeled FRV. However, the FRV structure does not appear in Figure 8 (the 25 km wavelength map) which indicates that contrasts in magnetization may not extend to the base of the magnetic crust. The two normal faults labeled C1 and C2 represent the western boundary of the High Cascades graben proposed by Allen (1965), and Taylor (1973, 1978). C1 and C2 are located at the transition from the high frequency to low frequency anomalies seen in Figures 5 and 7 and along a steep gradient in gravity anomalies (Pitts, 1979).

The normal fault labeled WR (Walker Rim) is interpreted from the prominent trend in Figure 8 (the low-pass filtered anomaly map with a cutoff wavelength of 25 km) oriented N 20° E and extending through the La Pine Valley. Although Lawrence (1976) proposes strike-slip motion along

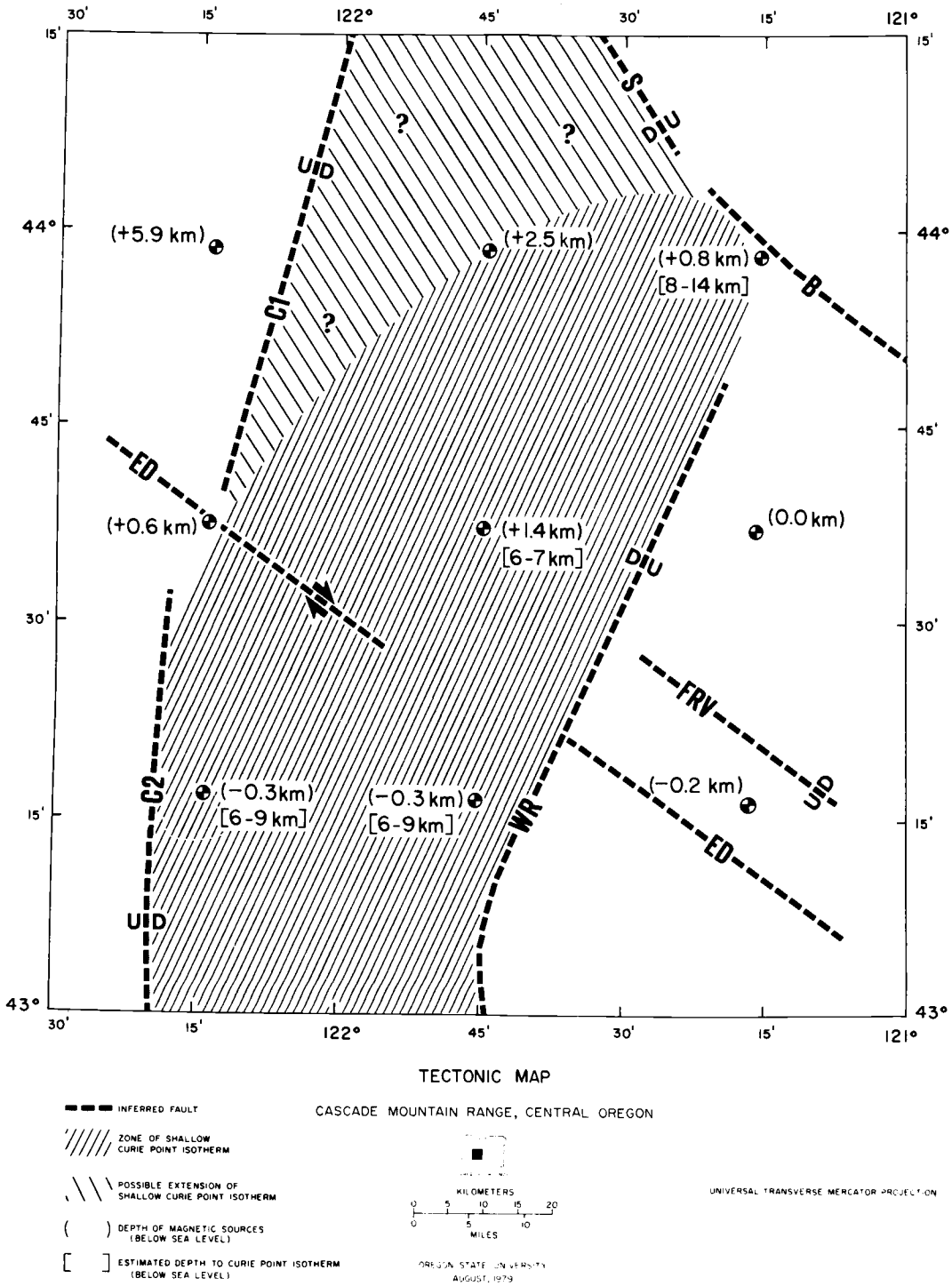

Figure 20. Map of the Central Oregon Cascades area showing areas of shallow Curie point isotherm and regional structural interpretation of aeromagnetic data.

the Eugene-Denio lineation and across the Walker Rim faults, the prominent Walker Rim faults show no evidence for this type of movement. Figures 5 and 7 also show a distinct truncation of the FRV and ED magnetic anomaly trends in the area of WR. This conjugate pattern of faulting appears to be a continuation of the Basin and Range pattern found southeast of the study area. On the basis of gravity data Pitts (1979) also proposed that the structural trends of the Basin and Range Province continue into the High Cascades.

The survey marks shown in Figure 20 locate the center of each of the nine subgrids. The numbers enclosed in parentheses are the deepest sources and those in brackets are the estimated Curie point isotherm depths, with sea level as zero depth. The source depths show a general trend from shallow in the south and southeast to deep in the northwest.

Depth-to-source computations on the northwest subgrid produce a significantly deeper source (6 km BSL) than any of the other subgrids. This is the only subgrid which is predominently over the Western Cascades province. A geologic cross section from Wells and Peck (1971) suggests a synclinal structure in this area with pyroclastic layers as deep as 6 km BSL. The relatively low heat flow for this area (Blackwell et al., 1978), is consistent with rocks at

this depth retaining contrast in magnetization large enough to be detected by this analysis.

The general shape of a zone of elevated Curie point isotherm depths is shown in Figure 20 enclosing the center of the four subgrids which give reliable Curie point depth estimates. The regional structure, and the heat flow data for this area reported by Blackwell et al. (1978) suggest that shallow Curie point depths extend to the north under the Three Sisters area. The lack of reliable Curie point depth estimates for the north subgrid may be related to the occurrence of source bodies with large horizontal dimensions in the Three Sisters-Lookout Mountain area.

Similar Curie depth calculations for other high heat flow areas in the Western U.S. give slightly deeper estimates. Smith et al. (1974) estimated a Curie point depth of 10±3 km BSL for the Yellowstone National Park area. Boler (1978) estimated a Curie point depth of 11.5±3 BSL for the Vale-Owyhee geothermal area of Eastern Oregon. However, the Curie point depths estimated for this area fit the thermal model of Blackwell et al. (1978) which predict a temperature of 600°C at a depth of 7.5 km under the High Cascades. Blackwell et al. (1978) also points out that in basin and range structures the highest temperatures at depth are likely to occur beneath the valleys, even though heat flow in the valleys may be slightly lower than in the ranges. The structural and subsurface thermal model

presented by this study and the thermal models of Blackwell et al. (1978) point to the High Cascades and the La Pine Valley as the most promising areas for further geothermal exploration.

The results of the depth-to-source computations and the Curie depth estimations in this study are consistent with the heat flow data and with other qualitative geologic information. However, the absolute numbers should be used with caution; they are estimates. The geologic and physiographic complexity of this area strain the assumptions of the interpretive models used in this study.

REFERENCES

Allen, J.E., 1965, The Cascade Range volcano-tectonic depression of Oregon: Trans. of the Lunar Geological Field Conference. Oregon Dept. Geo. Min. Indus., p. 21-23.

Baldwin, E.M., 1976, Geology of Oregon: Kendall/Hunt Publishing Co., Dubuque, Iowa. 147 pp.

Bhattacharyya, G.K. and Leu, L.K., 1974, Analysis of magnetic anomalies over Yellowstone National Park: mapping the Curie point isothermal surface for geothermal reconnaissance: J. Geophys. Res., V. 80, p. 4461-4465.

Bhattacharyya, B.K. and Morley, L.W., 1965, The delineation of deep crustal magnetic bodies from total field magnetic anomalies: J. Geomag. Geoelec., V. 17, p. 237-252.

Blackwell, D.D., Hull, D.A., Bowen, R.G. and Steele, J.L., 1978, Heat Flow of Oregon: Oregon Dept. Geo. Min. Indus. Special Paper 4.

Blakeley, R.J. and Hassanzedah, S., 1977, Depth to Magnetic Source and the Peru-Chile Trench: EOS, Trans. of the American Geophys. Union, V. 58, p. 1124.

Boler, F.M., 1978, Aeromagnetic Measurements, Magnetic Source Depths, and the Curie Point Isotherm in the Vale-Owyhee, Oregon: M.S. Thesis, Oregon State University, Corvallis.

Bowen, R.G., Peterson, R.G. and Riccio, J.F., 1978, Low-to-Intermediate Temperature Thermal Springs and Wells in Oregon: Oregon Dept. Geol. Min. Indus., Geological Map Series 10.

Bulina, L.V., 1961, The use of airborne magnetic prospecting data in deep-seated structure of the earth's crust within the Siberian platform: Sovetskaya Geo Geologiya, V. 5, p. 134-138.

Byerly, P.E. and Stolt, R.H., 1977, An attempt to define the Curie point isotherm in northern and central Arizona: Geophysics, V. 42, p. 1394-1400.

Callaghan, E. and Buddington, A.F., 1938, Metaliferous mineral deposits of the Cascade Range in Oregon: U.S. Geol. Survey Bull. 893, 144 p.

Dicken, S.N., 1965, Oregon Geography: Eugene, Oregon. 4th ed., 127 p.

Donath, F.A., 1958, Basin and Range Structures of South-central Oregon: Ph.D. Thesis, Stanford University, Palo Alto, California. 144 p.

Donath, F.A., 1962, Analysis of Basin-and-Range Structure, South-central Oregon: Geol. Soc. of America Bull., V. 73, p. 1-16.

Gasparini, P., Mantovani, M.S.M., Corrado, G. and Rapolla, A., 1979, Depth of Curie Temperature in Continental Shields: A Compositional Boundary?: Nature, V. 278, p. 845-846.

Goodwin, L.H., Haigler, L.B., Rious, R.L., White, D.E., Muffler, L.J.P., and Wayland, R.G., 1971, Classification of Public Lands Valuable for Geothermal Steam and Associated Geothermal Resources: U.S. Geol. Survey Circular #67, 18 p.

Gudmundsson, G., 1967, Spectral analysis of magnetic surveys, Geophys. J.R. astr. Soc., 18, 325-337.

Haggarty, S.E., 1978, Mineralogical constraints on Curie isotherms in deep crustal magnetic bodies: Geophys. Res. Letters, V. 5, p. 105-108.

Hall, D.H., 1968, Regional magnetic anomalies, magnetic units, and crustal structure in the Kenora District of Ontario: Can. J. earth Sci., V. 5, p. 1277-1296.

Lawrence, R.D., 1976, Strike slip faulting terminates the Basin and Range province in Oregon: Geol. Soc. Am., V. 87, p. 846-850.

MacLeod, N.S., Walker, G.W., McKee, E.H., 1975, Geothermal Significance of Eastward Increase in Age of Upper Cenozoic Rhyolitic Domes in Southeast Oregon: (U.S. Geol. Survey Open-file Report 75-348), 2nd U.N. Symp. on the Development of Geothermal Resources, San Francisco, California, 1975, p. 465-474, U.S. Govt. Printing Office, Washington, D.C.

McBirney, A.R., 1968, Petrochemistry of Cascade Andesite Volcanoes: In Andesite Conference Guidebook, Editor: H.M. Dole, Oregon Dept. Geol. Min. Indus. Bull 62, p. 101-107.

Mishra, D.C. and Naidu, P.A., 1974, Two-dimensional Power Spectral Analysis of Aeromagnetic Fields: Geophs. Prosp., V. 22, p. 345-353.

Naidu, P., 1969, Estimation of the spectrum and cross spectrum of aeromagnetic field using fast digital Fourier transform (FDFT) techniques: Geophs. Prosp., V. 17, p. 344-361.

Naidu, P., 1970, Statistical structure of aeromagnetic field: Geophys., V. 35, p. 279-292.

Peck, D.L., Griggs, A.B., Schlicker, H.D., Wells, F.G., Dole, H.M., 1964, Geology of the Central and Northern Part of the Western Cascade Range in Oregon: U.S. Geol. Survey Prof. Paper 449, U.S. Govt. Printing Office, Washington, D.C.

Peterson, N.V., and Groh, E.A., 1963, Maars of South-Central Oregon: The Ore Bin, V. 24, no. 5, p. 73-88.

Peterson, N.V. and McIntyre, J.M., 1970, The Reconnaissance Geology and Mineral Resources of Eastern Klamath County and Western Lake County, Oregon: Oregon Dept. Geol. Min. Indus., Bull. 66, 70 p.

Peterson, N.V., Groh, E.A., Taylor, E.M. and Stensland, D.E., 1976. Geology and Mineral Resources of Deschutes County, Oregon: Oregon Dept. Geol. Min. Indus., Bull. 89, 66 p.

Pitts, G.S., 1979, Interpretation of Gravity Measurements Made in the Cascade Mountains and the Adjoining Basin Range Province in Central Oregon: M.S. Thesis, Oregon State University, Corvallis.

Scholz, C.H., Barazangi, M., and Sbar, M.L., 1971, Late Cenozoic Evolution of the Great Basin, Western United States, as an Ensialic Interarc Basin: Geol. Soc. Am. Bull., V. 82, p. 2979-2990.

Shuey, R.T., Schellinger, D.K., Tripp, A.C. and Alley, L.B., 1977, Curie depth determination from aeromagnetic spectra: Geophys. J.R. Astr. Soc., V. 50, p. 75-102.

Smith, R.B., 1977, Intraplate Tectonics of the Western North American Plate: Tectonophysics, V. 37, p. 323-336.

Smith, R.B., Shuey, R.T., Freidline, R.O., Otis, R.M., and Alley, L.B., 1974, Yellowstone hot spot: new magnetic and seismic evidence: Geology, V. 2, p. 451-455.

Spector, A., 1968, Spectral analysis of aeromagnetic data: Ph.D. Dissertation, University of Toronto, Toronto, Canada.

Spector, A. and Grant, F.S., 1970, Statistical models for interpreting aeromagnetic data: Geophysics, V. 35, p. 293-302.

Stacey, F.D., 1977, Physics of the Earth: John Wiley and Sons, New York, N.Y., 2nd ed., 414 p.

Taylor, E.M., 1973, Geology of the Deschutes Basin: Geologic Field Trips in Northern Oregon and Southern Washington: Oregon Dept. Min. Indus. Bull. 77, p. 28-32.

Taylor, E.M., 1978, Field Geology of S.W. Broken Top Quadrangle, Oregon: Oregon Dept. Geol. Min. Indus. Special Paper 2.

Tsuboi, C. and Fuchida, T., 1937, Relation between gravity values and corresponding subterranean mass distribution: Bull. Earth Res. Inst. Tokyo, V. 15, p. 636-649.

Treitel, S., Clement, W.G. and Kaul, R.K., 1971, The Spectral Determination of Depths to Buried Magnetic Basement Rocks: Geophys. J.R. Astr. Soc., V. 24, p. 415-428.

Wasilweski, P.J., Thomas, H.H., and Mayhew, M.A., 1979, The Moho as a Magnetic Boundary: Geophys. Res. Letters, V. 6, p. 541-544.

Wells, F.G. and Peck, D.L., 1961, Geologic Map of Oregon West of the 121st Meridian: Oregon Dept. Geol. Min. Indus. in coop. with the U.S. Geol. Survey.

Williams, H., 1957, A geologic map of the Bend Quadrangle, Oregon and a Reconnaissance Geologic Map of the Central Portion of the High Cascade Mountains: Oregon Dept. Geol. Min. Indus. in coop. with the U.S. Geol. Survey.

Walker, G.W., 1969, Geology of the High Lava Plains province: Oregon Dept. Geol. Min. Indus. in coop. with the U.S. Geol. Survey, Bull. 64, p. 77-79.

APPENDICES

APPENDIX A

Previous Geophysical Work

Previous aeromagnetic surveys in and near the southern portion of this study area are surveys by Scintrex (1972), Geometrics (1973), and a small survey flown over Mt. Matzama (Blank, 1968). The Geometrics survey which covered most of the Medford AMS sheet, extended from 42° to 43°N latitude and from 122° to 124°30'W longitude and used an average flight line spacing of two miles. The Scintrex survey covered the area from 42° to 43°30'N latitude and from 120° to 122°W longitude and also used a two mile spacing. The Scintrex survey used a fluxgate magnetometer which gave total magnetic intensity readings relative to an arbitrary datum. In the area of overlap with this current study, the anomalies from the Scintrex map are the same general shape but have less detail. Using data from the Geometrics and Scintrex surveys in the Klamath Falls region, Van Deusen (1978) attempted to map the relative depth of the Curie point isotherm in a qualitative way. He suggested that areas of negative magnetic anomalies represent shallow Curie point isotherms.

Paleomagnetic studies by Heinrichs (1973) and Champion (1979) near and in the area, examined the secular variation of the main geomagnetic field using recent volcanic flows. The range of inclinations, declinations, and remanent magnetic intensities are listed in Table A1. A

Table A1. Summary of paleomagnetic data from 36 flows in the Cascades Range of Central Oregon.

	Number of Flows Sample	Inclination (degree)			Declination (degree)			J_{NRM} (emu/cm^3)		
		Min.	Average	Max.	Min.	Average	Max.	Min.	Average	Max.
Heinrichs	9	45.2	52.6	64.8	354.8	3.5	17.9	5.48×10^{-3}	1.12×10^{-2}	1.88×10^{-2}
Champion	27	44.7	57.8	73.0	342.1	357.6		2.92×10^{-4}	9.72×10^{-3}	2.03×10^{-2}

magnetotelluic traverse of Oregon (Bodvarsson et al., 1974) indicated values typically observed in mafic Tertiary volcanics (Bodvarsson, 1950) for the station located at Sisters, Oregon, just north of the study area.

Seismicity within the study area is low. In a review of earthquake activity in Oregon, Couch and Lowell (1971) show only one epicenter in the area (near Bend) and state that the Cascade Range is relatively quiet seismically. However, just south and east of this study, Donath (1958, 1962) and Donath and Kuo (1962) carried out a detailed seismic survey of basin and range faulting in the Summer Lake area. Donath clearly identified two major fault trends, one oriented about N 20° to 30°E and the other N 30° to 40°W. This pattern has been traced over the entire Basin and Range province in Oregon using ERTS-1 images (Lawrence, 1976) and extends up to and across the High Cascades Range.

Pitts (1979) established 933 new gravity stations which he combined with data from Woollard and Rose (1963), Blank (1965, 1966, 1968), Thiruvathukal (1968), Leutsher (1968), and Griscom (1974, 1975) to construct free-air, complete Bouguer, and residual gravity anomaly maps of this study area. In his analysis of the maps, Pitts found that the structural trends of the Basin and Range Province continue into the High Cascade Range and that a graben-like structure may exist under the High Cascades.

Blackwell et al. (1978) summarized the heat-flow data for Oregon. Their heat-flow map of the state shows a steep heat-flow gradient at the boundary between the Western and High Cascade Range, with heat-flow values greater than 100 mW/m^2 found in the High Cascades and Basin and Range portions of the study area. However, reliable heat flow data are not available for the central and eastern parts of the High Cascade Range.

REFERENCES

Blackwell, D.D., Hull, D.A., Bowen, R.G. and Steele, J.L., 1978, Heat Flow of Oregon: Oregon Dept. of Geol. and Min. Indus. Special Paper 4.

Blank, H.R., Jr., 1965, Southwest Oregon Gravity Data: U.S. Geol. Survey Open-File Report, 63 computer print-out sheets, 1 p., 1 map, scale 1:250,000.

Blank, H.R., Jr., 1966, General Features of the Bouguer Gravity Field in Southwestern Oregon: U.S. Geol. Survey Prof. Paper 550-C, U.S. Govt. Printing Office, Washington, D.C.

Blank, H.R., 1968, Aeromagnetic and Gravity Surveys of Crater Lake Region, Oregon: Andesite Conference Guide-book, Editor: H.M. Dole, Oregon Dept. Geol. Min. Indus., Bull. 62, p. 42-52.

Bodvarsson, G., 1950, Geophysical methods in the prospect-ing of hot water in Iceland: J. Eng. Assoc. (Iceland), V. 35, no. 5, p. 49-59.

Bodvarsson, G., Couch, R.W., MacFarlane, W.T., Tang, R.W. and Whitsett, R.M., 1974, Telluric Current Exploration for Geothermal Anomalies in Oregon: The Ore Bin, V. 36, no. 6, p. 93-107.

Champion, D., 1979, Holocene Geomagnetic Secular Variation in the Western U.S.: Implications for the Global Geomagnetic Field: Ph.D. Dissertation, California Institute of Technology, Pasadena.

Couch, R.W. and Lowell, R.P., 1971, Earthquakes and seismic energy release in Oregon: The Ore Bin, V. 33, no. 4, p. 61-84.

Donath, F.A., 1958, Basin and Range Structures of South-central Oregon: Ph.D. Thesis, Stanford University, Palo Alto, California.

Donath, F.A., 1962, Analysis of Basin-and-Range Structure, South-central Oregon: Geol. Soc. of America, Bull., V. 73, p. 1-16.

Donath, F.A. and Kuo, J.T., 1962, Seismic-refraction study of Block Faulting, South-central Oregon: Geol. Soc. America Bull., V. 73, p. 429-434.

Geometrics, Inc., 1973, Aeromagnetic Map of the Medford Sheet, Oregon: U.S. Geol. Survey Open-File Report, 1:250,000.

Griscom, A., 1974, Wart Peak Gravity Survey: Unpub. data, U.S. Geol. Survey, Menlo Park, California.

Griscom, A., 1975, Newberry Crater Gravity Survey: Unpub. data, U.S. Geol. Survey, Menlo Park, California.

Heinrichs, D.F., 1973, Paleomagnetic Study of Recent Cascade Lavas, Three Sisters, Oregon: J. Geoph. Res., V. 18, p. 5983-5992.

Lawrence, R.D., 1976, Strike-slip Faulting Terminates Basin and Range Province in Oregon: Geol, Soc. of Am. Bull., V. 87, p. 846-850.

Leutsher, J., 1968, Newberry Crater Gravity Survey: Unpub. data, U.S. Geol. Survey, Menlo Park, California.

Pitts, G.S., 1979, Interpretation of Gravity Measurements Made in the Cascade Mountains and Adjoining Basin Range Province in Central Oregon: M.S. Thesis, Oregon State University, Corvallis.

Scintrex Mineral Surveys, Inc., 1972, Aeromagnetic Map of the Klamath Falls and Crescent Sheets, Oregon: U.S. Geol. Survey Open-File Report, 1:250,000.

Thiruvathukal, J.T., 1968, Regional Gravity of Oregon: Ph.D. Dissertation, Oregon State University, Corvallis.

Van Deusen, J.E., III, 1978, Mapping Geothermal Anomalies in the Klamath Falls, Oregon Region with Gravity and Aeromagnetic Data: M.S. Thesis, University of Oregon, Eugene.

Woollard, G.P., Rose, J.C., 1963, International gravity measurements: Society of Exploration Geophysics, Tulsa, OK, 518 p.

APPENDIX B

The Central Cascades Aeromagnetic Survey Data Collection

During October and November, 1976, personnel from the Geophysics Group at Oregon State University made preparations for the aeromagnetic survey of the Central Cascades region. Concurrent with a geophysical study of the Vale-Owyhee geothermal area (Boler, 1978), an aircraft was modified and equipment installed for aeromagnetic surveying. Gemperle and Bowers (1977) give a complete description of the aeromagnetic survey techniques and equipment used.

A Motorola Mini-Ranger III navigation system, consisting of two ground-based radar transponders and a receiver-transmitter and system console in the aircraft, provided horizontal position control for the survey. The control module in the survey airplane interrogated the transponders and determined the range from each transponder every five seconds. With a long range 19db sector antenna used on the transponders, a maximum range of 75 kilometers with a resolution of ±3 meters was possible. The accuracy of the fix calculated from the two ranges varied over the area of the survey as a function of the angle of intersection of the two antenna patterns. For the Central Cascades survey area the error gain factor varied from one to about five resulting in average positional accuracy for the plane of approximately 10 meters. In the worst case, in the fringes

of the transponder coverage, the error in horizontal position was less than 30 meters.

The transponders were placed over, or within, a hundred meters in some cases, of a geodetic triangulation station. The State Plane Coordinates and the latitude and longitude of the triangulation stations obtained from the U.S. Coast and Geodetic Survey and based on the North American Datum of 1927 (Swick, 1932), gave the horizontal coordinates for the transponders to 0.1 ft. for transponders placed on the triangulation stations and 1 ft. for locations surveyed in the field. The vertical coordinate in both cases is known to within 5-10 ft. However, because the solution to the equation determining the air plane's horizontal position is not sensitive to errors in elevation, the vertical uncertainty does not increase the horizontal position uncertainty.

An additional consideration is the 300 milli-second delay between a fix and the corresponding magnetic reading. Flying at 225 km/hr with the sensor about 20 meters behind the plane, the magnetic data are obtained at the navigational fix position. Variations in aircraft ground speed cause errors of less than 5 meters in the location of the magnetic measurement. Therefore, the total average positional accuracy of the data is 15 meters.

There were short intervals in some flights where unacceptable fixes occurred because of occasional signal

transmission problems due to the effects of weather or terrain on the transponder navigation system. Interpolation between good fixes along the flight lines increased the total number of usable data points by about 5%.

To provide piloting information for real-time control of the aircraft, the Mini-Ranger console transmitted the range information to a Hewlett Packard HP-97 calculator which was programmed to calculate the offset distance from the desired flight line less than 10 seconds after receipt of a good fix. This system enabled the pilot to keep the airplane within 15 meters of the desired flight line horizontally in smooth weather.

In addition to the navigation system, the integrated aeromagnetic system included a Geometrics model G-801/3 proton precession magnetometer with a 100 ft. towing cable, a Rosemont pressure altimeter, and a Bonzer radar altimeter. The acquisition system recorded the total magnetic field measurement, altitude, ranges from the Mini-Ranger, and time of the measurement every five seconds on a Digi-Data 7-track incremental tape recorder at 200 bpi (bits per inch).

During the entire survey, a base station located near the center of the survey area at Sunriver, Oregon, recorded the outputs of a Varain proton precession magnetometer and a Rosemont pressure altimeter on magnetic tape and strip charts. This base station data provided dirunal

corrections for both the magnetic and pressure altitude measurements. Base station personnel continuously monitored the base station magnetometer and geomagnetic field activity forecasts from the Center in Boulder, Colorado, to identify periods of extreme geomagnetic field activity.

During the course of the survey, logistical problems caused two minor relocations of the base station. Figures B1, B2 and B3 show histograms of magnetic values obtained at the three base stations. The modal value of the entire recording period at each base station established the "base reference value" (regional field plus anomaly at the base station) to be used for the diurnal magnetic corrections at the particular base station.

Data Processing

Preliminary processing of the raw data from the aircraft data acquisition system consisted of screening the magnetic tapes for data errors and converting the navigation ranges to State Plane Coordinates and latitude and longitude. Base station tapes were also checked for data errors and smoothed using a five-point moving average. Next, magnetic anomalies were calculated, using the following equation:

$$A = M(t) - D(t) - R$$

where A is the anomaly, M is the measured value of the

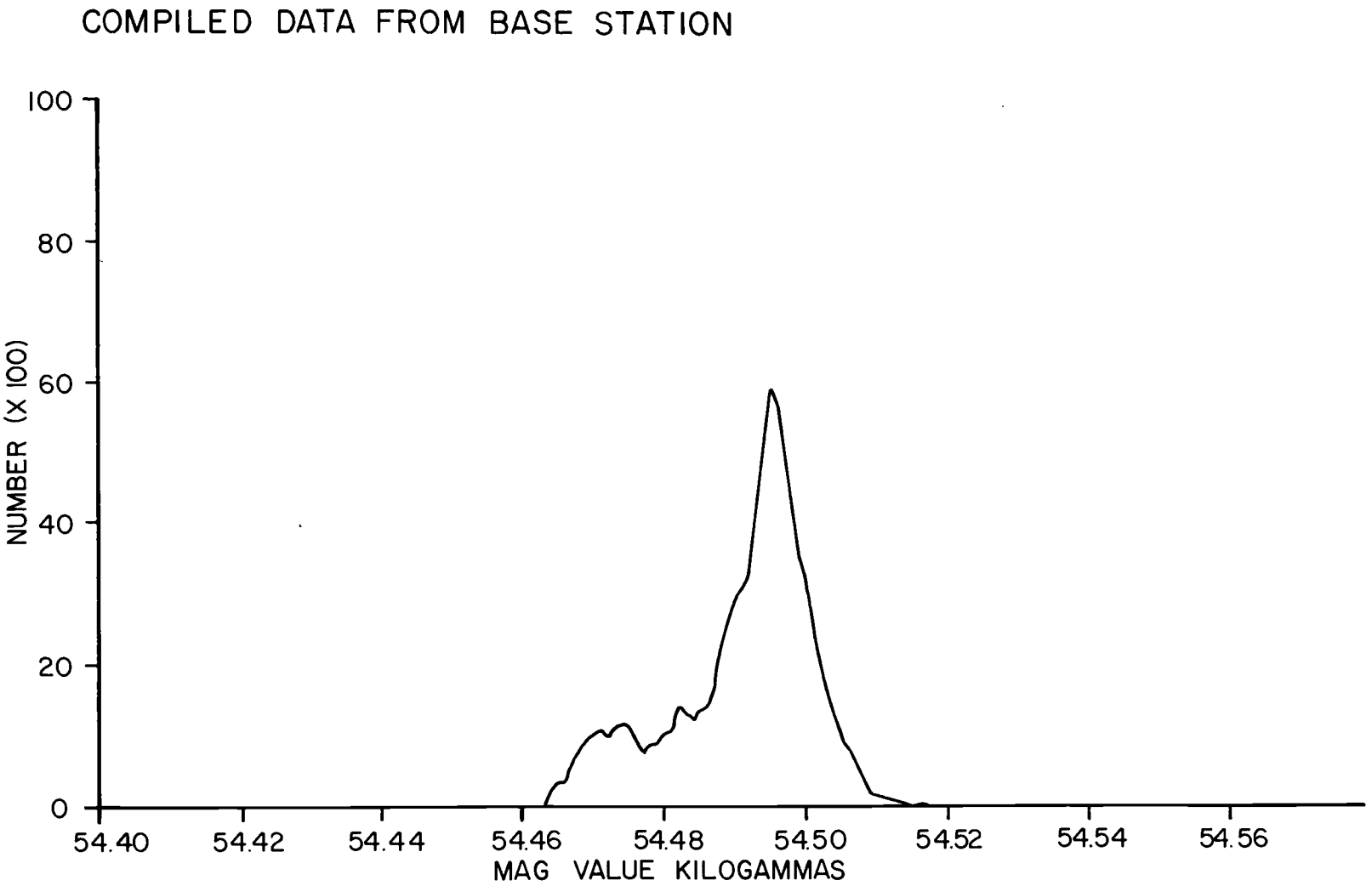

Figure B1. Histogram of magnetic values recorded at the Sunriver base station #1 from 9 May to 14 May 1977.

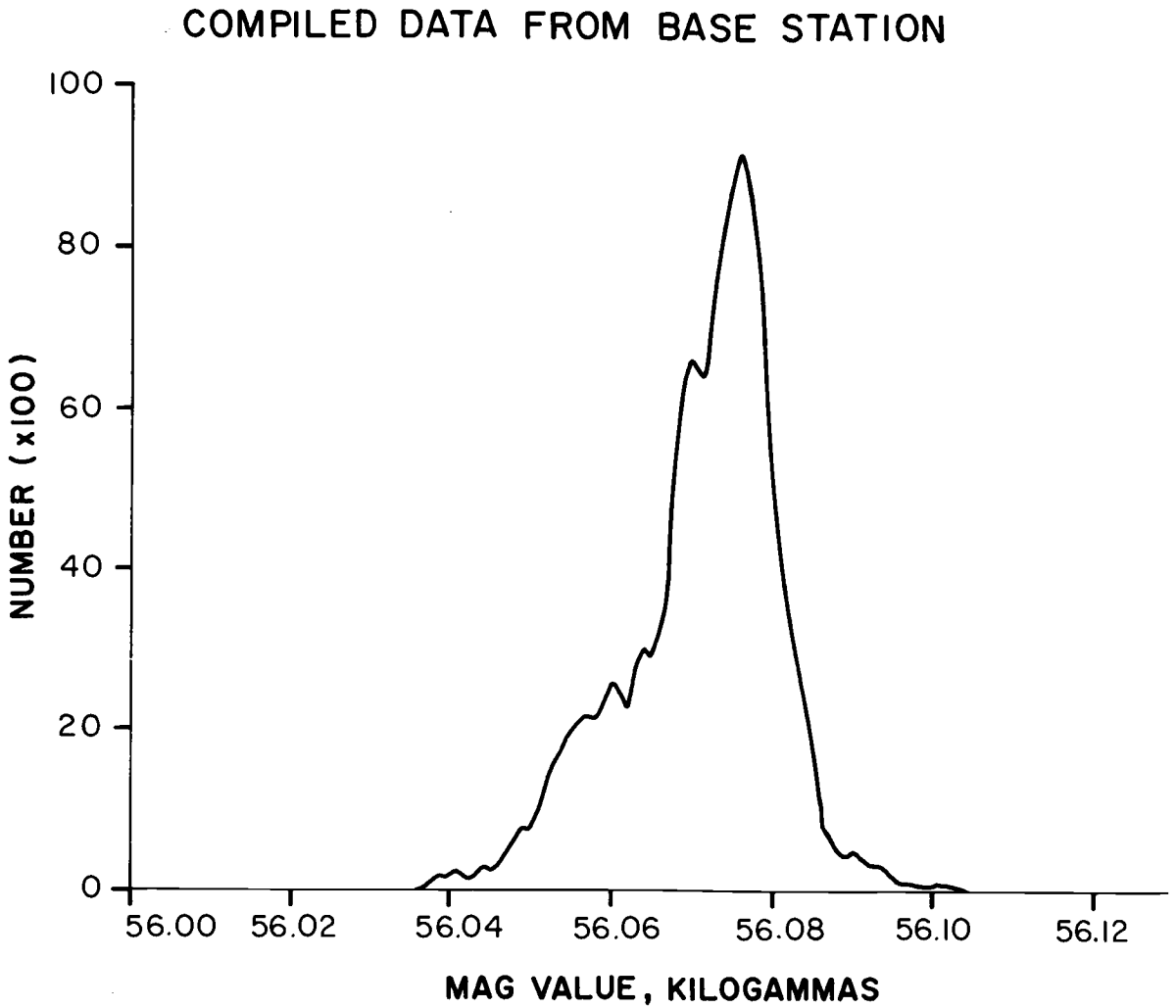

Figure B2. Histogram of magnetic values recorded at the Sunriver base station #2 from 14 May to 15 June 1977.

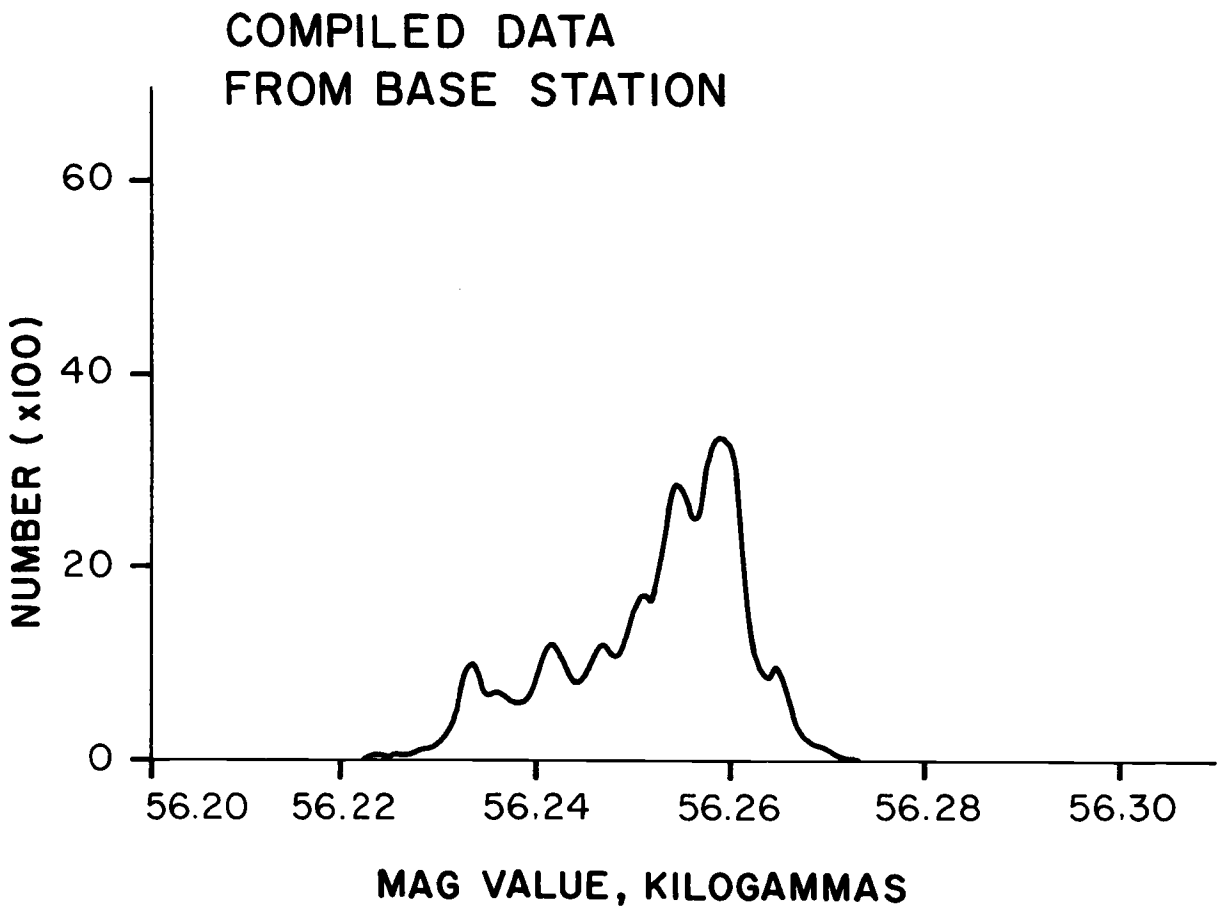

Figure B3. Histogram of magnetic values recorded at the Sunriver base station #3 from 15 June to 25 June 1977.

total magnetic field at time t, D is the diurnal variation at time t, and R is the regional magnetic field. The total field value measured at the base station at time t minus the base reference value yields the diurnal magnetic variation D(t). The regional magnetic field R was determined from the International Geomagnetic Reference Field of 1975 (International Association of Geomagnetism and Aeromagnetism, 1976) updated to the survey time. The following equations represent planes fit to the IGRF at the survey elevations to reduce the computational effort required to calculate regional field values at each data point:

$$R_{11000}(x,y) = 52045.4 + (8.8209 \times 10^{-4})x + (1.3520 \times 10^{-3})y,$$

$$R_{9000}(x,y) = 52061.9 + (8.8252 \times 10^{-4}) + (1.3521 \times 10^{-3})y,$$

where x and y are in State Plane Coordinates. The values determined from the equations above agree with the values computed from the IGRF to within 4 gammas for the entire survey area. This stage of data processing produced approximately 60,000 usable data points.

A simple statistical analysis of the differences at survey line and tie line crossings yielded an estimate of the RMS uncertainty of the final magnetic anomaly values. A careful examination of the flight line misties indicated small but systematic differences between the three "base reference values" initially used for the survey. Two of

the reference values were adjusted (one by 7 gammas, the other by 2 gammas) to minimize the differences and the corresponding anomaly values were recalculated for the final version of the analysis and map preparation. Figure B4 is a histogram of 1,416 crossing errors calculated for the lines flown at 9,000 ft. ASL. Table B1 lists the corresponding statistics. The RMS uncertainty per line attributes one half of the mistie to each of the flight lines used in calculating the uncertainty, i.e.,

$$\text{RMS uncertainty per line} = \text{RMS mistie}/\sqrt{2}$$

Figure B5 is a histogram of the 86 crossing errors calculated for the lines flown at 11,000 ft. ASL in the Three Sisters area. Table B2 lists the corresponding statistics. The mode is -1γ in Figure B4 and 2γ in Figure B5. These low uncertainties reflect the excellent navigation control and the careful monitoring of diurnal changes. Estimates of the components of the uncertainty are as follows:

1γ - resolution of airborne magnetometer

1γ - resolution of base station magnetometer

1-2γ - diurnal correction

1-2γ - x-y position determination in low gradient areas

1-2γ - z position determination

Approximately 46,000 magnetic measurements made at 9,000 ft. were used in the preparation of the larger map shown in Figure 5, and 3,200 measurements made at 11,000 ft. were

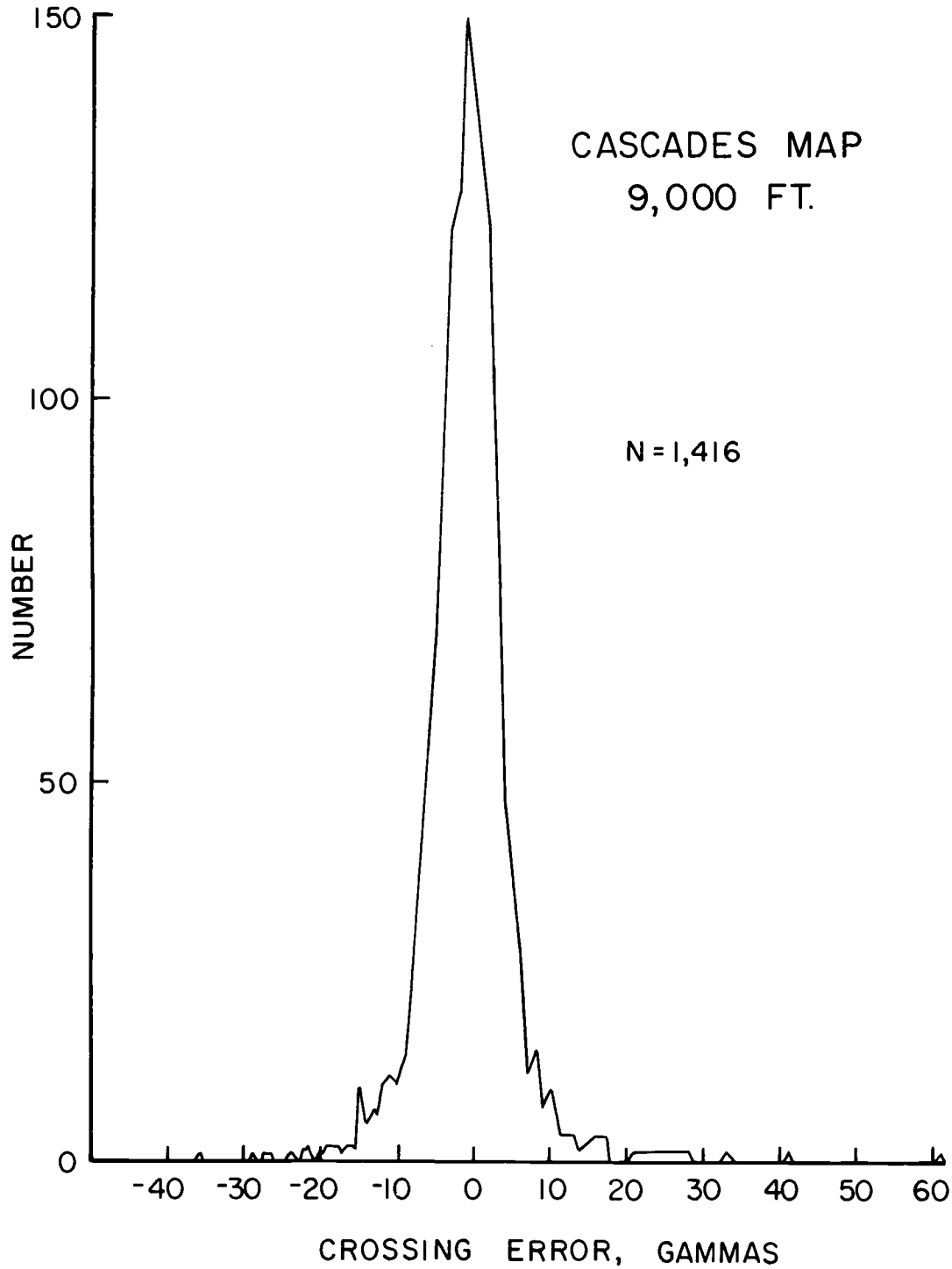

Figure B4. Histogram of the crossing errors for the 9,000 ft. ASL survey.

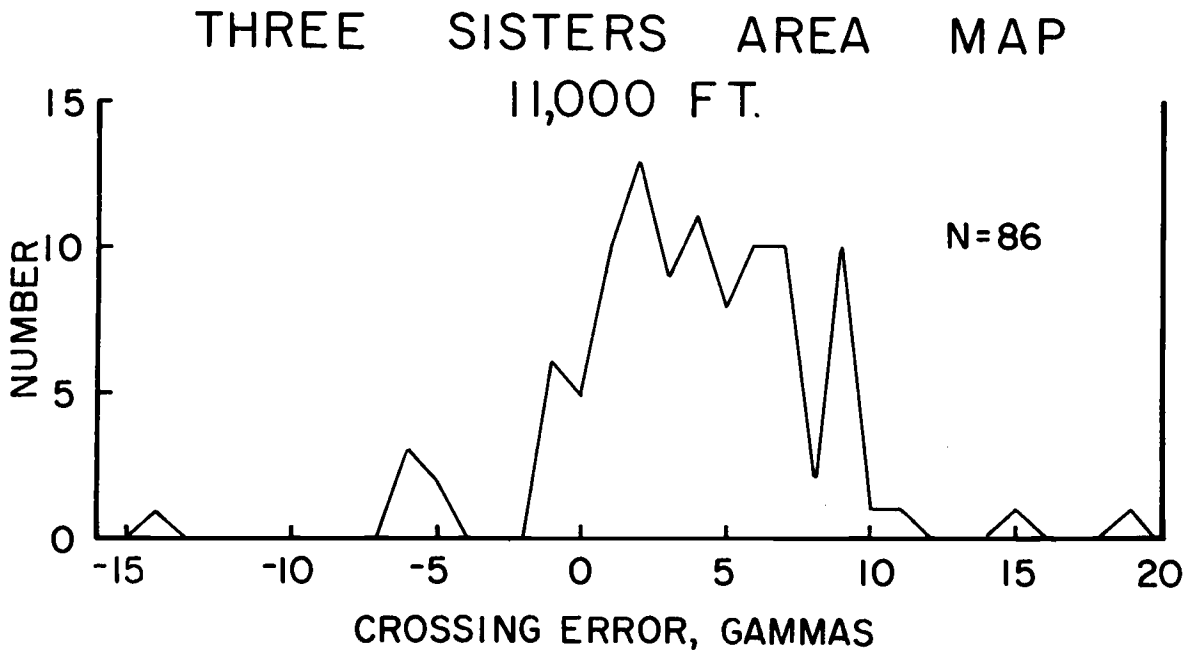

Figure B5. Histogram of the crossing errors for the 11,000 ft. ASL survey.

Table B1. Cascades 9,000 ft. ASL survey crossing error statistics.

Total crossings	1,416
Mean	Ø
Median	-1
Mode	-1
RMS	5.9
RMS uncertainty per line	4.2

Table B2. Three Sisters area 11,000 ft. ASL survey crossing error statistics.

Total crossings	86
Mean	3
Median	3
Mode	2
RMS	5.4
RMS uncertainty per line	3.8

used in the Three Sisters area map shown in Figure 6. The remainder of the 60,000 measurements were essentially duplications and were not used in the final plots. Flights were plotted at a scale of 1:62,500 for hand contouring and then reduced by 1/2 to 1:125,000 for drafting. Gemperle et al. (1978) give a detailed description of the aeromagnetic data processing computer programs and formulae.

REFERENCES

Boler, F.M., 1978, Aeromagnetic Measurements, Magnetic Source Depths, and the Curie Point Isotherm in the Vale-Owyhee Oregon: M.S. Thesis, Oregon State University, Corvallis.

Gemperle, M., and Bowers, J.E., 1977, Aeromag in a Mooney: Geophysics technical report number 770301, Oregon State University, Corvallis.

Gemperle, M., Connard, G.C., Keeling, K.K. and Boler, F.M., 1978, Aeromagnetic data processing: Geophysics technical report number 780401, Oregon State University, Corvallis.

International Association of Geomagnetism and Aeronomy, 1976, International Geomagnetic Reference Field 1975: EOS, Transactions of the American Geophysical Union, V. 57, p. 120-121.

Swick, C.H., 1932, First and second order triangulation in Oregon: U.S. Dept. of Commerce, Coast and Geodetic Survey Special Publication number 75.

APPENDIX C

Techniques of Analysis of the Central Cascade Aeromagnetic Data

Quantitative analyses of aeromagnetic data generally include the solution of either the direct or the inverse problem. The solution of the direct problem involves the calculation of the theoretical anomaly for a given model and relies on curve-matching or fitting of characteristic curves. The solution of the inverse problem calculates the parameters of the causative structures directly from the anomalies.

In recent years, various researchers have published a large number of techniques for the solution of the inverse problem using spectral approaches. The spectral analysis approach involves the study of the anomalies in terms of their wavelength or frequencies. Bhattacharyya (1966) derived an expression for the continuous spectrum of the magnetic anomalies associated with a rectangular prismatic body. Spector (1968) discussed four operations for which spectral analysis is useful in aeromagnetic data interpretations: (1) depth to source interpretations; (2) filtering out high frequency anomalies from near surface sources to enhance deeper sources; (3) continuation of the field observed at one level to another level; and (4) "rotation-to-the-pole" for determining what the anomalies would be if they were caused by the same sources with vertical

magnetization measured in a vertical field. Spector and Grant (1970) transformed Bhattacharyya's expression for the spectrum into polar coordinates and developed a technique for determining the mean depths of ensembles of bodies from the energy spectrum of the magnetic anomalies. Mishra and Naidu (1974) used similar techniques to analyze aeromagnetic maps. Shuey et al. (1977) and Bhattacharyya and Leu (1975) extended these methods with emphasis on determining the lower boundaries of source bodies. These boundaries may be interpreted as the Curie point isotherm depths, or depths at which rocks lose their magnetization due to high temperature. Information about the Curie isotherm depths adds important constraints on the assessment of the geothermal potential of an area.

This study applies methods similar to those used by Spector and Grant (1970) and Shuey et al. (1977) for determining source depths and Curie point isotherm depths using the Central Cascades aeromagnetic data. This study also utilizes low-pass filtering techniques in the frequency domain as described by Spector (1968). The first step in these methods is the transformation of the data from the space domain to the wave number domain using a two-dimensional Fourier Transform.

Two-Dimensional Fourier Transform

If $f(x,y)$ represents the aeromagnetic data as a function of spatial position, the two-dimensional Fourier

transform of f(x,y) is

$$F(u,v) = \int_{-\infty}^{\infty}\int_{-\infty}^{\infty} f(x,y)e^{-i2\pi(ux+vy)}dxdy$$

and the inverse Fourier transform is

$$f(x,y) = \frac{1}{4\pi^2}\int_{-\infty}^{\infty}\int_{-\infty}^{\infty} F(uv,)e^{i2\pi(ux+vy)}dudv$$

where u and v are the spatial frequencies in cycles per unit distance in the x and y directions respectively. The Fourier transform F(uv,) is, in general, complex and contains information about the amplitude and phase relationships of all the frequencies that make up the function f(x,y).

For the case of aeromagnetic data sampled at discrete, even intervals (Δx and Δy) and over the finite sample area (Lx by Ly), the Fourier transform becomes the Discrete Fourier transform (DFT):

$$F(u,v) = \sum_{n=o}^{Nx-1}\sum_{m=o}^{Ny-1} f(m\Delta x,\ n\Delta y)e^{-2\pi(um\Delta x\ +\ vn\Delta y)}$$

(Kanasewich, 1975, p. 44) where Nx and Ny represent the number of sampled points in the x and y directions, Δx = Lx/(Nx-1) and Δy = Ly/(Ny-1). In the frequency domain, the sample intervals are

$$\Delta u = 1/(Nx\Delta x) \quad \text{and} \quad \Delta v = 1/(Ny\Delta y)$$

The requirements that the spectrum of the data be sampled

at discrete points can result in aliasing or shifting of high frequency components of the anomaly field into the lower frequencies. For aeromagnetic maps, Spector (1968) suggests choosing the sample spacing such that Δx and Δy are no greater than one-quarter of the width of the sharpest magnetic features in the mapped anomalies to avoid aliasing problems.

The finite size of aeromagnetic surveys also dictates that only an estimate of the true spectrum can be obtained. The mapped anomalies are a "boxcar" window through which only a part of the total magnetic field is observed. In the frequency domain, the sharp edges of the "boxcar" function causes a large amount of distortion at frequencies higher than 4π/width of the survey area (Spector, 1968). To minimize these boundary effects, this study applied a "cosine bell" window (Kanasewich, 1976) which tapers 10% of the data at the edge of the survey area to zero using a cosine function.

The Fourier transform of the total field magnetic anomaly of a vertical sided rectangular prism with horizontal top and bottom (derived by Bhattacharyya, 1966) is:

$$F(u,v) = 2\pi M e^{-h(u^2+v^2)^{\frac{1}{2}}}(1-e^{-t(u^2+v^2)^{\frac{1}{2}}})S(u,v)R_p(u,v)R_G(u,v)$$

where M = magnetic moment/unit depth

h = depth to the top of the prism

t = thickness of the prism

S = factor for horizontal size of the prism

R_p = factor for magnetization direction of the prism

R_G = factor for geometric field direction

The terms involving the geomagnetic field and magnetization directions are separate factors which can be divided out of the expression and replaced by multiplying by factors for observation in a vertical magnetic field (at the magnetic pole) and for vertical magnetization to perform the rotation-to-pole operation described by Spector (1968). The operation is the same for multiple causative bodies if the field direction and magnetization direction are assumed to be constant.

Low-pass filtering to study the magnetic effects of deep crustal bodies consists of multiplying the anomaly map, transformed to the frequency domain, by a weighting function $\bar{W}$ where

$$\bar{W}(u,v) = 1 \qquad u^2 + v^2 \leq r_o$$

$$\bar{W}(u,v) = 0 \qquad u^2 + v^2 > r_o$$

and r_o is the desired cutoff frequency. The high frequency distortion caused by this simple "boxcar" weighting does not seriously affect the low frequency anomalies of interest.

Mean Depth-to-Source Boundaries From the Energy Spectrum

Spector (1968) described the energy spectrum E(u,v) of the magnetic anomaly as:

$$E(u,v) = F(u,v) \cdot F^*(u,v)$$

where * indicates the complex conjugate. Transcribing the energy spectrum into polar wavenumber coordinates in the u,v frequency plane gives:

$$E(r,\theta) = 4\pi^2 M^2 e^{-2hr}(1-e^{-tr})S^2(r,\theta)R_p^2(\theta)R_G^2(\theta)$$

where $r = (u^2+v^2)^{\frac{1}{2}}$ and $\theta = \tan^{-1}(u/v)$. Spector and Grant (1970) assumed that the sources of the anomalies in an aeromagnetic anomaly map are a number of independent ensembles of rectangular prismatic blocks. Each ensemble was assumed to be characterized by a joint frequency distribution for the depth h, thickness t, width a, length b, and the direction of the magnetization. Over a region the size of this survey the geomagnetic field direction does not vary appreciably so that $R_G(\theta)$ is constant. The energy spectrum thus becomes:

$$\left\langle E(r,\theta)\right\rangle = 4\pi^2 M^2 R_G^2 \left\langle e^{-2hr}\right\rangle \left\langle (1-e^{-tr})^2\right\rangle \left\langle R_p^2(\theta)\right\rangle \left\langle S^2(r\cdot\theta)\right\rangle$$

where $\langle\ \rangle$ indicates the expected value from an ensemble of

vertical prism sources. Taking the average with respect to θ gives:

$$\left\langle \bar{E}(r) \right\rangle = 4\pi^2 M^2 R_G^2 \left\langle \bar{R}_p^2 \right\rangle \left\langle (1-e^{-tr})^2 \right\rangle \left\langle \bar{S}^2(r) \right\rangle \left\langle e^{-2hr} \right\rangle$$

where $\bar{E}$, $\bar{R}$, and $\bar{S}$ indicate the average over θ.

Notice that the ensemble average depth $\bar{h}$ only appears in the factor $\left\langle e^{-2hr} \right\rangle$. Spector (1968) shows that for $\Delta h/\bar{h} < .25$, $\left\langle e^{-2hr} \right\rangle = e^{-2\bar{h}r}$. Spector and Grant (1970) state that the $e^{-2\bar{h}r}$ term is invariably the dominating factor in the energy spectrum and show a number of aeromagnetic surveys that exhibit two distinct ensembles of sources at two mean depths.

Because the longest wavelength for which the Fourier transform can be calculated is the total length of the mapped area, the spectrum of the area only contains meaningful depth information down to $L/2\pi$ (Shuey et al., 1977; Regan and Hinze, 1976) where L is the length of longest side of the mapped area. If the area is large enough that the low frequency anomalies caused by the lower boundary of sources are included, the factor $(1-e^{-tr})^2$ in combination with the factor e^{-2hr} introduces a peak or maximum in the spectrum which shifts toward longer wavelengths with increasing values to t. If most of the magnetic bodies in the area extend deeper than $L/2\pi$, the spectral peak occurs at $r = 0$ and cannot be seen at all.

The location of the spectral peak is also influenced by the depth of the top of the source. Figure C1 shows families of depth-to-bottom vs. depth-to-top values for which the spectral peak is located at the same frequency. In general

$$f_{max} = \frac{1}{2\pi(d-h)} \ln \frac{d}{h}$$

where h is the depth to the top of the source, d is the depth to the bottom of the source, and f_{max} is the spacial frequency of the spectral peak. For thin bodies with h = d the relationship above reduces to $f_{max} = \frac{1}{2\pi}$. However, thin bodies require an unreasonably large value of magnetization. Shuey et al. (1977) suggest that source bodies need to be a minimum of 5 km thick, a value used in this study to give an upper limit for depth-to-bottom estimates.

The horizontal dimensions of the sources represented by the shape factor S also affect the spectrum. As the horizontal dimensions increase, the short wavelength side of the spectrum is depressed and the spectral peak moves slightly towards longer wavelengths. Spector and Grant (1970) give the shape factor as

$$S(r,) = \frac{\sin(a \cdot r \cdot \cos\theta)}{a \cdot r \cdot \cos\theta} \cdot \frac{\sin(b \cdot r \cdot \cos\theta)}{v \cdot r \cdot \cos\theta}$$

for a rectangular body whose dimensions are 2a x 2b. Shuey et al. (1977) show that for a body with horizontal dimensions comparable to the survey area, the spectral maximum

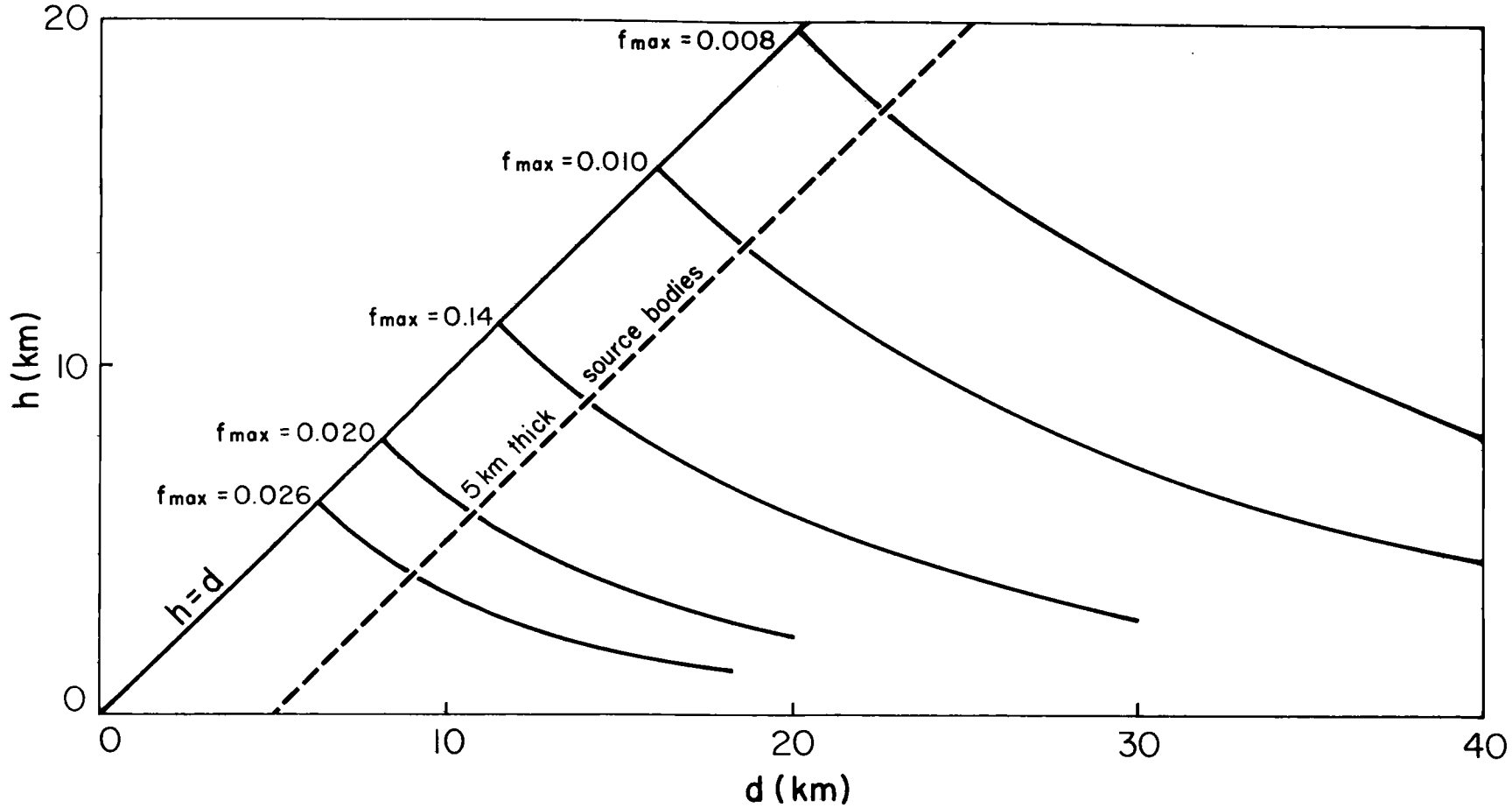

Figure C1. Families of curves of depth-to-bottom of the source vs. depth-to-top of the source.

is displaced to zero frequency. Because a regional anomaly gradient would be indistinguishable from such a body, anomalies need to be detrended before computing the spectrum. Therefore spectral peaks, consisting of one point occurring at the fundamental frequency, are inadequate for calculating Curie point depths.

REFERENCES

Bhattacharyya, B.K., 1966, Continuous spectrum of the total magnetic field anomaly due to a rectangular prismatic body: Geophysics, V. 31, p. 97-212.

Bhattacharyya, B.K. and Leu, L.K., 1975, Analysis of magnetic anomalies over Yellowstone National Park: mapping the Curie Point Isothermal surface for geothermal reconnaissance: J. Geophys. Res., V. 80, p. 4461-4465.

Kanasewich, E.R., 1976, Time Sequence Analysis in Geophysics, Second Revised Edition: Edmonton, Alberta, Canada, University of Alberta Press.

Mishra, D.C. and Naidu, P.A., 1974, Two-dimensional Power Spectral Analysis of Aeromagnetic Fields: Geoph. Prosp., V. 22, p. 345-353.

Regan, R.D. and Hinze, W.J., 1976, The effect of finite data length in the spectral analysis of ideal gravity anomalies: Geophysics, V. 41, p. 44-45.

Shuey, R.T., Schellinger, D.K., Tripp, A.C. and A-ley, L.B. 1977, Curie depth determination from aeromagnetic spectra: Geophys. J.R. Astr. Soc., V. 50, p. 75-102.

Spector, A., 1968, Spectral analysis of aeromagnetic data: Ph.D. Diss., University of Toronto, Canada.

Spector, A. and Grant, F.S., 1970, Statistical models for interpreting aeromagnetic data: Geophysics, V. 35, p. 293-302.

APPENDIX D

Computer Processing Considerations

The computer algorithm used in this study for two-dimensional fast Fourier transforms (FFT) is from Brenner (1968) and requires that the data be spaced at equal intervals on a grid with 2^n grid points in each direction. The algorithm by Briggs (1975) was used to interpolate the flight line data onto an equally spaced grid by minimizing the curvature of a surface through the value at the grid points. Listings and documentation for the gridding and FFT programs appear in Boler et al. (1978) and Pitts (1979).

Figure 9 shows the boundaries of the grid relative to the flight line data which provided the input to the gridding program. The average data spacing along the flight lines, 305 meters (1,000 ft.), dictated the grid spacing in both the x (E-W) and y (N-S) directions. With this grid spacing a 512 x 512 grid covered the entire survey area, with a border of 18 grid points outside both the east and west edges. The 512 x 512 grid is a composite of four smaller grids of the NE, NW, SW and SE quadrants of the area, divided at approximately 43°37.5'N latitude and 121°45'W longitude. To provide agreement at the boundaries, the four subgrids had dimensions of 261 x 261 so that adjacent grids overlapped each other by 10 grid points. After gridding, the five outermost points along the common

boundaries were removed, leaving each subgrid with dimensions of 256 x 256 and no overlap with adjacent grids. The two external boundaries of each quadrant grid were set to zero before gridding to allow the minimum curvature gridding program to bring the outer edges of the 512 x 512 grid smoothly to zero. After gridding, and before applying the Fourier transform, the grid was detrended by fitting a plane to the grid by least-squares using program DETREND which is described at the end of this appendix. To remove any offsets at the edges of the grid, a border of 10 grid points along the outside edge of the grid was tapered using a cosine bell window by program GRIDTAPER which is described below.

Program RADPLOT calculated the radial average of the natural logarithm of the energy spectrum and produced the plots shown in Figures 10-19. It averages the squared amplitude or energy of each element (m,n) of the complex two dimensional frequency domain array generated by the FFT operation. One point on the plot represents the average of all elements within a ring of Δf wide. The 8 elements with $0.5 < (m^2+n^2)^{\frac{1}{2}} \leq 2.5$ are averaged for the third point; and so forth. The zero frequency element (m=0, n=0), which is the first point on the plot, is not averaged with any other element. Boler (1979) describes RADPLOT in detail, and also the program RADSLOPE used to fit the lines to the spectra shown in Figures 10-19.

To prepare the nine subgrids used in the detailed analysis, program GRIDSTRIP was used to extract the desired 256 x 256 subgrid and program GRIDTAPER was then used to taper 10 grid points around the border of the grid smoothly to zero. Documentation for GRIDSTRIP appears below.

DETREND

The input to program DETREND is a random access file containing a square grid of magnetic anomaly measurements. DETREND asks the user for the grid dimensions. Any size grid up to 512 x 512 is allowed. DETREND fits a surface to the gridded data using least-squares and subtracts the surface from the input grid to yield a detrended grid. The outputs are a random access file containing the detrended grid and a listing of the trend coefficients on the user terminal.

GRIDSTRIP

GRIDSTRIP reads a random access file containing a 512 x 512 grid and extracts a specified 256 x 256 grid. The location of the 256 x 256 grid to be extracted is specified by giving the indices of the grid point which is one point closer to the origin than the first point to be included in the output grid. The origin is at the southwest corner of the grid.

GRIDTAPER

The input to program GRIDTAPER is a random access file containing a square grid of magnetic anomaly measurements. The program asks the user for the grid dimensions. Any size grid up to 512 x 512 is allowed. GRIDTAPER applies a ten point cosine taper to all four of the boundaries of the grid. The outermost grid points are set to zero; the next tier is reduced by a factor of .0245; and so forth.

```
     DETREND                    10/11/79   9:13:54     PAGE  1
 1;C  PROGRAM DETREND
 2;C
 3;C  TO FIT A FIRST ORDER SURFACE TO AN INPUT GRID,
 4;C  REMOVE THE SURFACE AND OUTPUT A DETRENDED GRID
 5;C  AND TREND COEFFIIENTS
 6;C
 7;C  19 MAY 78 GSP - MODIFIED FOR ANY SIZE GRID .LE. 512 JULY 79 GGC
 8;
 9;       DIMENSION GRD(512), S(3,3), G(3), B(3)
10;C  SET IO
11;       IOIN = 1
12;       IOUT = 2
13;       IOW  = 10
14;       IOR  = 11
15;     1 ACCEPT 'GIVE GRID SIZE ',NX
16;       IF(NX.LE.512) GO TO 2
17;       TYPE 'GRID SIZE .GT. 512 - TRY AGAIN'
18;       GO TO 1
19;     2 NX4=4*NX
20;       NY=NX
21;C  SET S, G, B
22;       DO 10 I = 1, 3
23;       G(I) = 0.0
24;       B(I) = 0.0
25;       DO 10 J = 1, 3
26;       S(J,I) = 0.0
27; 10    CONTINUE
28;C  SET S(1,1)
29;       S(1,1) = FLOAT(NX) * FLOAT(NY)
30;C  OPEN FILES
31;       CALL PIN  ( IOIN, NX4, 9H OLD GRID )
32;       CALL POUT ( IOUT, NX4, 10H DETRENDED )
33;C  FOR NY PROFILES
34;       DO 50 IY = 1, NY
35;C  SET Y
36;       Y = FLOAT (IY)
37;       Y2 = Y * Y
38;C  READ ONE PROFILE
39;       CALL READR ( IOIN, IY, GRD, 1, IER )
40;C  FOR NX POINTS PER PROFILE
41;       DO 40 IX = 1, NX
42;C  SET X, Z
43;       X = FLOAT (IX)
44;       Z = GRD (IX)
45;       X2 = X * X
46;       XY = X * Y
47;C  DO SUMS
48;       S(1,2) = S(1,2) + X
49;       S(2,2) = S(2,2) + X2
50;       S(3,2) = S(3,2) + XY
51;       S(1,3) = S(1,3) + Y
52;       S(3,3) = S(3,3) + Y2
53;       G(1) = G(1) + Z
54;       G(2) = G(2) + Z * X
55;       G(3) = G(3) + Z * Y
56;C  NEXT  POINT
57; 40    CONTINUE
58;C  NEXT PROFILE
```

```
      DETREND                    10/11/79   9:13:54      PAGE  2
 59; 50    CONTINUE
 60;       TYPE ' END READ SEQUANCE '
 61;C  FILL IN THE ARRAY
 62;       S(2,1) = S(1,2)
 63;       S(3,1) = S(1,3)
 64;       S(2,3) = S(3,2)
 65;C  CALCULATE TREND COEFFICENTS
 66;       DO 56 K = 1, 3
 67;       SKK = S(K,K)
 68;       S(K,K) = 1.0
 69;       DO 52 J = 1, 3
 70;       S(K,J) = S(K,J) / SKK
 71; 52    CONTINUE
 72;       DO 56 I = 1,3
 73;       IF (I-K) 54,56,54
 74; 54    SIK = S(I,K)
 75;       S(I,K) = 0.0
 76;       DO 56 J = 1,3
 77;       S(I,J) = S(I,J) - SIK * S(K,J)
 78; 56    CONTINUE
 79;       DO 58 I = 1,3
 80;       DO 58 J = 1,3
 81;       B(I) = B(I) + S(I,J) * G(J)
 82; 58    CONTINUE
 83;C
 84;       TYPE ' BEGIN DETREND '
 85;C  DETREND GRID
 86;C
 87;C  FOR NY PROFILES
 88;       DO 70 IY = 1, NY
 89;       Y = FLOAT (IY)
 90;C  READ ONE PROFILE
 91;       CALL READR ( IOIN, IY, GRD, 1, IER )
 92;C  FOR NX POINTS PER PROFILE
 93;       DO 60 IX = 1, NX
 94;       X = FLOAT (IX)
 95;C  CALCULATE TREND
 96;       TREND = B(1) + B(2) * X + B(3) * Y
 97;C  DETREND THIS POINT
 98;       GRD(IX) = GRD(IX) - TREND
 99;C  NEXT POINT
100; 60    CONTINUE
101;C  OUTPUT NEW PROFILE
102;       CALL WRITR ( IOUT, IY, GRD, 1, IER )
103;C  NEXT PROFILE
104; 70    CONTINUE
105;C  AND TO TTY
106;       WRITE ( IOW, 90 ) B(1), B(2), B(3)
107; 90    FORMAT ( '0TREND (X,Y) = ',F6.2,' + ',F6.2,' * X + ',F6.2,' * Y ')
108;C  CLEAN HOUSE
109;       CALL RESET
110;       STOP
111;       END
```

```
     GRIDSTRIP                  10/11/79   9:13:54      PAGE  1
 1;C  PROGRAM GRIDSTRIP
 2;C  TO READ A 512 X 512 GRID AND EXTRACT A 256 X 256 GRID FROM
 3;C  SPECIFIED FIRST PROFILE AND POINT
 4;C  28 AUG 78 GSP MODIFIED 10/02/78 FMB - MOD 1/10/79 GGC
 5;C
 6;       PARAMETER NX=256, NY=256, NX2=512, NX4=1024, NXP=512,NXP2=1024
 7;       PARAMETER NXP4=2048
 8;       DIMENSION A1(NXP2), A2(NX)
 9;       COMMON IA1(NX4), IA2(NX2)
10;       EQUIVALENCE ( A1, IA1 ), ( A2, IA2 )
11;C  SET PARAMETERS
12;       IO1 = 1
13;       IO2 = 2
14;    10 ACCEPT "LAST EXCLUDED POINT FROM SW: ",NXOFF
15;       ACCEPT "LAST EXCLUDED PROFILE FROM SW: ",NYOFF
16;       NXD=NXF-NXOFF
17;       NYD=NXF-NYOFF
18;       IF(NXD.GE.NX.AND.NYD.GE.NY)GO TO 20
19;       TYPE NXD," X ",NYD," GRID NOT ALLOWED,TRY AGAIN"
20;       GO TO 10
21;C  OPEN FILES
22;    20 CALL PIN ( IO1, NXP4, 9H  NXPGRID )
23;       CALL POUT ( IO2, NX4, 9H  128GRID )
24;C  FOR NY PROFILES IN THE NEW GRID
25;       DO 50 IY = 1, NY
26;       JY = IY + NYOFF
27;C  READ ONE PROFILE
28;       CALL READR ( IO1, JY, IA1, 1, IER, NB )
29;C  FOR NX POINTS IN EACH NEW PROFILE
30;       DO 40 IX = 1, NX
31;       JX = IX + NXOFF
32;       A2(IX) = A1(JX)
33;  40   CONTINUE
34;C  WRITE OUT NEW PROFILE
35;       CALL WRITR ( IO2, IY, IA2, 1, IER, NB )
36;  50   CONTINUE
37;C  CLEAN HOUSE
38;       CALL RESET
39;       STOP
40;       END
```

```
     GRIDTAPER                10/11/79   9:13.54      PAGE  1
 1;C      PROGRAM GRIDTAPER
 2;C      CONNARD 1/30/79
 3;C      APPLIES A 10 POINT COSINE TAPER TO THE EDGES OF ANY GRID .LE. 512X512
 4;C
 5;       DIMENSION GRID(512)
 6;       COMMON /DUM/ IGRID(1024),CT(10)
 7;       EQUIVALENCE (GRID(1),IGRID(1))
 8;       DATA CT(1)/0.,.0245,.0955,.2061,.3455,.500,.6545,.7939,.9045,.9755/
 9;     1 ACCEPT 'GIVE GRID SIZE ',NX
10;       IF(NX.LE.512) GO TO 2
11;       TYPE 'GRID SIZE .GT. 512 - TRY AGAIN'
12;       GO TO 1
13;     2 NX4=4*NX
14;       NY=NX
15;       CALL PIN(1,NX4,7HIN GRID)
16;       CALL POUT(2,NX4,7HOUTGRID)
17;C  DEAL WITH THE FIRST 10 PROFILES
18;       DO 10 IY=1,10
19;       CALL READR(1,IY,IGRID(1),1,IER,NB)
20;       IF(IER.NE.1) TYPE IER
21;       IX1=IY-1
22;       NXX=NX-IY+1
23;       DO 5 IX=IY,NXX
24;    5  GRID(IX)=GRID(IX)*CT(IY)
25;       DO 6 IX=1,IX1
26;       GRID(IX)=GRID(IX)*CT(IX)
27;       IX2=NX-IX +1
28;     6 GRID(IX2)=GRID(IX2)*CT(IX)
29;       CALL WRITR(2,IY,IGRID(1),1,IER,NB)
30;       IF(IER.NE.1) TYPE 'WRITE ERR ',IER
31;    10 CONTINUE
32;C  PROFILES 11 THRU IY-10
33;       IYM10=NY-10
34;       DO 20 IY=11,IYM10
35;       CALL READR(1,IY,IGRID(1),1,IER,NB)
36;       IF(IER.NE.1) TYPE IER
37;       DO 15 IX=1,10
38;       IX2=NX-IX+1
39;       GRID(IX)=GRID(IX)*CT(IX)
40;    15 GRID(IX2)=GRID(IX2)*CT(IX)
41;       CALL WRITR(2,IY,IGRID(1),1,IER,NB)
42;       IF(IER.NE.1) TYPE 'WRITE ERR ',IER
43;    20 CONTINUE
44;C  PROFILES NY-9 THRU NY
45;       NYM9=NY-9
46;       DO 30 IY=NYM9,NY
47;       CALL READR(1,IY,IGRID(1),1,IER,NB)
48;       IF(IER.NE.1) TYPE IER
49;       IX1=NX-IY+1
50;       DO 12 IX=IX1,IY
51;    12 GRID(IX)=GRID(IX)*CT(IX1)
52;       IX1=NX-IY
53;       DO 16 IX=1,IX1
54;       GRID(IX)=GRID(IX)*CT(IX)
55;       IX2=NX-IX+1
56;    16 GRID(IX2)=GRID(IX2)*CT(IX)
57;       CALL WRITR(2,IY,IGRID(1),1,IER,NB)
58;       IF(IER.NE.1) TYPE 'WRITE ERR ',IER
```

```
      GRIDTAPER                  10/11/79   9:13:54     PAGE  2
59;   30 CONTINUE
60;      CALL RESET
61;      STOP
62;      END
```

REFERENCES

Boler, F.M., 1978, Aeromagnetic Measurements, Magnetic Source Depths, and the Curie Point Isotherm in the Vale-Owyhee, Oregon Geothermal Area: M.S. Thesis, Oregon State University, Corvallis.

Boler, F.M., Pitts, G.S., Connard, G.G., and Gemperle, M., 1978, Geophysics technical report, Number 781215: Oregon State University, Corvallis.

Brenner, N., 1968, FOR2D subroutine package for two dimensional FFT: MIT Lincoln Laboratory, Boston.

Briggs, I.C., 1975, A program to contour using minimum curvature: Australia Bureau of Mineral Resources, Geology and Geophysics, Department of Energy and Minerals, report 1975/98.

Pitts, G.S., 1979, Interpretation of gravity measurements made in the Cascade mountains and the adjoining Basin and Range province in central Oregon: M.S. Thesis, Oregon State University, Corvallis.